

AD-A101 396

SOIL CONSERVATION SERVICE, OXFORD MS SEDIMENTATION LAB F/0 5/8
STREAM CHANNEL STABILITY. APPENDIX K. TWO-DIMENSIONAL FINITE-ELEMENT--ETC(U)
APR 81 T SU, S WANG

ML

UNCLASSIFIED

For I
A
401-598

END
DATE
8-81
DTIC

AD A101396

LEVEL III

①

STREAM CHANNEL STABILITY

APPENDIX K

TWO-DIMENSION FINITE-ELEMENT MODEL FOR ROUTING WATER AND SEDIMENT IN SHORT ALLUVIAL CHANNEL REACHES

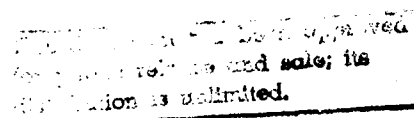
Project Objective 4

by

T. Y. Su and S. Y. Wang

*USDA Sedimentation Laboratory
Oxford, Mississippi*

April 1981



*Prepared for
US Army Corps of Engineers, Vicksburg District
Vicksburg, Mississippi*

*Under
Section 32 Program, Work Unit 7*

DTIC
ELEC.
S JUL 15 1981
D

FILE
DTIC

81 7 14 096

STREAM CHANNEL STABILITY.

APPENDIX K

TWO-DIMENSIONAL FINITE-ELEMENT MODEL FOR
ROUTING WATER AND SEDIMENT IN SHORT
ALLUVIAL CHANNEL REACHES

Project Objective 4

by

Tsu-Yi Su ~~Su~~ and Shu-Yi Wang ~~Wang~~

USDA Sedimentation Laboratory

Oxford, Mississippi

April 1981

Bell

Prepared for

US Army Corps of Engineers, Vicksburg District
Vicksburg, Mississippi

Under

Section 32 Program, Work Unit 7

- 1/ Research Associate, Department of Mechanical Engineering, The University of Mississippi, University, MS.
- 2/ Associate Professor, Department of Mechanical Engineering, The University of Mississippi, University, MS.

412456

PREFACE

The main objective of this study is to develop a two-dimensional numerical model capable of studying water and sediment movement and geomorphic changes in alluvial channel reaches with complex geometries. A description of the governing equations for water and sediment motion in two dimensions is presented in Part 2 of this report. Part 3 presents a detailed description of the numerical methods used to discretize the governing equations so that the solution can be carried out with the aid of a digital computer. Part 4 of this report presents results of applications of the model to the prediction of a trench scour and fill, and the simulation of bed scour around a spur dike.

Accession For	
NTIS GRA&I	<input checked="" type="checkbox"/>
DTIC TAB	<input type="checkbox"/>
Unannounced	<input type="checkbox"/>
Justification	
Per form 50 On file	
By _____	
Distribution	
Availability Codes	
Avail and/or	
Dist	Special
A	

TABLE OF CONTENTS

	<i>Page</i>
List of Figures	3
U.S. Customary to S.I.-Units Conversion Factors	4
1 Introduction	5
2. Formulation of Mathematical Model	8
2.1 Equations of Water Movement	8
2.2 Equations of Sediment Movement	14
3 Numerical Solutions	19
3.1 Depth-Averaging Model	19
3.2 Two-Dimensional Vertical Flow Model	22
4 Presentation and Examination of Results	26
4.1 Flow Around a Spur Dike in a Straight Channel with a Sand Bed .	26
4.2 Local Scour and Fill of a Trench in a Sand Bed Stream	34
5 Conclusions and Recommendations	39
5.1 Conclusions	39
5.2 Recommendations	39
References	41
Addendum 1. Derivation of Two-Dimensional Depth-Averaged Flow Equations	45
Addendum 2. Computer Program of Depth-Averaged Flow Model	48

LIST OF FIGURES

Figure	Page
1. The coordinate system	11
2. A typical finite element grid using quadrilateral elements . . .	20
3. Sketch of finite element grid at $t = 0$	23
4. Dimensions of straight channel with spur dike	27
5. Velocity distribution around spur dike after 5 hours	28
6. Velocity distribution around spur dike after 10 hours	29
7. Velocity distribution around spur dike after 15 hours	30
8. Bed deformation around spur dike after 5 hours	31
9. Bed deformation around spur dike after 10 hours	32
10. Bed deformation around spur dike after 15 hours	33
11. Sketch of finite element grid at $t > 0$	35
12. Evolution of free-surface and bed profiles	37
13. Distribution of suspended sediment after 7 hours	38

U.S. Customary to S.I.-Units Conversion Factors

To convert	To	Multiply by
inches (in.)	millimeters (mm)	25.4
feet (ft)	meters (m)	0.305
yards (yd)	meters (m)	0.914
miles (miles)	kilometers (km)	1.61
square inches (sq. in.)	square millimeters (mm^2)	645
square feet (sq ft)	square meters (m^2)	0.093
square yards (sq yd)	square meters (m^2)	0.836
square miles (sq miles)	square kilometers (km^2)	2.59
acres (acre)	hectares (ha)	0.405
cubic inches (cu in.)	cubic millimeters (mm^3)	16,400
cubic feet (cu ft)	cubic meters (m^3)	0.028
cubic yards (cu yd)	cubic meters (m^3)	0.765
pounds (lb) mass	kilograms (kg)	0.453
tons (ton) mass	kilograms (kg)	907
pound force (lbf)	newtons (N)	4.45
kilogram force (kgf)	newtons (N)	9.81
pounds per square foot (psf)	pascals (Pa)	47.9
pounds per square inch (psi)	kilopascals (kPa)	6.89
U.S. gallons (gal)	liters (L)	3.79
acre-feet (acre-ft)	cubic meters (m^3)	1,233

INTRODUCTION

The objective of this study is to develop a new methodology for modeling the phenomenon of sediment movement in irregular alluvial channels, scouring around obstructions, etc. The basic physical principles of conservation of mass and momentum are used to describe the fluid flow. The conservation of mass and semi-empirical equations governing sediment particle movement are adopted to establish the interaction between the sediment movement and the fluid flow. The resulting mathematical model is, unfortunately, highly nonlinear and complex. It is impractical, if not impossible, to solve it analytically. Therefore, the numerical methods of finite element and finite difference are used to obtain approximate solutions of this model.

The application of the finite element method (FEM) to model fluid flows has progressed rapidly in recent years from the simplest linear inviscid fluid flow problems (Martin, 1968; Argyris et al., 1969) to slow viscous flows (Tong, 1969; Atkinson et al., 1969; Oden and Sornogyi, 1969), and finally to the solution of the full Navier-Stokes equations (Oden, 1970; Skiba, 1970; Olson, 1972; Oden and Wellford, 1972). However, this latter area represents an extremely large and complex field. As such, the research, although very active, can only be referred to as being in its beginning stage (Olson, 1975). A summary of its recent applications to flows through porous media, shallow water circulation, and two-dimensional viscous flows had been presented by Connor and Brebbia (1976). Norrie and de Vries (1978) also presented an excellent survey of the FEM applications in all branches of fluid mechanics with 218 papers cited. Readers, desiring to find detailed information on the development of FE Modeling of Fluid Flows in general, are referenced to these and other similar papers. A complete review on FE Modeling of Open Channel Flows and directly related works is presented below.

A variational principle for an ideal fluid flow with a free surface under gravity was developed by Luke (1967) using potential function formulation. It was modified using the stream function formulation and the different expressions of free surface boundary conditions by O'Carroll (1975), and by O'Carrol et al. (1976). O'Carrol (1975a, 1978) also applied this FEM to compute the flows by a vertically two-dimensional model and

over a spillway, etc. Although he only solved the problems without the effects of side walls; he contributed a great deal to techniques for handling the moving free surface at least for the ideal fluid flow. Using the Galerkin's approach of the FEM, Keuning (1976) solved a straight horizontal channel with a uniform trapezoidal cross section. Although the problem is only one-dimensional, the equations are kept nonlinear and unsteady.

A two-dimensional quasi-linear FE Model for Open Channel Flow near Critical Conditions was reported recently by Katopodes (1980). It successfully demonstrated the capability of FEM to simulate a supercritical floodwave. The truly three-dimensional finite element modeling of viscous flows in an open channel with and without the existence of obstructions was carried out by Alonso and Wang (1978). Three-dimensional linear hexahedral, isoparametric elements were used to obtain very slow viscous laminar flows in open channels of varying cross-section and around an isolated obstruction. Although results obtained were physically sound and mathematically reasonable, the requirement of computer storage and computing time were prohibitive. One of the most effective alternatives is the depth-averaging scheme. It has been used primarily in the simulation of currents and water waves in lakes, estuaries and shallow coastal water. Some typical contributions may be found in Leendertse (1967), Nakayama and Romero (1971), and Niemeyer (1977). More recently the utilization of the depth-averaging models in the finite element simulation of flows in open channels and rivers were reported by Thienpont and Berlamont (1980) and Wang, Su, and Alonso (1980). Because the distribution of hydrodynamic properties in the vertical direction of a shallow water flow are usually better understood, appropriate functions can, thus, be chosen to yield adequate approximation in this direction. Therefore, the governing differential equations can be integrated vertically from the channel bed to the free surface resulting in differential equations, containing vertically averaged properties, which are only two-dimensional in a horizontal reference plane. Even if the time derivatives are retained in the equations to model unsteady flows, the requirement of computer storage as well as computing time to simulate an open channel flow is greatly reduced. Besides, this approach not only gives reasonable results with adequate accuracy, but allows better resolution in horizontal directions by using

the computer storage saved from reducing three-dimensional to two-dimensional formulation to add more nodes on a horizontal plane. Furthermore, the computer code developed based on this approach has the potential of wider acceptance by users with limited computing resources. The simulation of sediment transport is discussed below.

In recent years one-dimensional, mathematical models of sediment routing, morphological transients, and sediment deposition, etc. were developed (Cunge and Perdreau, 1973; Mahmood, 1974; Simons et al., 1975; Lopez, 1978). Although they do not provide the time-varying configuration of the sand bed in a horizontal plane, these models contribute a great deal in understanding the basic characteristics of morphological transients as well as in estimating the sediment discharge at various locations of waterway system. A large number of contributions in the area of sediment transport in suspension has been published in recent years using the numerical techniques to solve the sediment convection-diffusion equation in a vertical plane. Some typical examples may be found in Jobson and Sayre (1970), Yang and Sayre (1971), and Chen (1971). Smith and O'Connor (1977) and Kerssens, et al. (1977) presented their findings at the 17th Congress of IAHR. The former paper described a two-dimensional model in a vertical plane which gives the velocity, as well as the concentration fields, of an estuarial type flow with only good agreement with experimental data of the velocity distribution. The latter paper succeeded in combining the quasi-steady fluid flow equations, sediment continuity equation, and the convection-diffusion equation for morphological computations in a vertical plane of a very wide alluvial channel. Some of its basic assumptions are adopted from an early work of deVries (1973). Their numerical estimation of sand bed deformation considering only sediment transport in suspension compares quite well with their own experimental results. These two models are based on finite-difference schemes. Leimkuhler et al. (1975), and Ariathurai et al. (1976) applied the FEM to obtain solution of the sediment convection-diffusion equation in a vertical plane with some success. Most recently, Alonso and Wang (1980) presented the results of a study of local scour and fill in sand bed stream. The bed deformation is verified with experimental results. This latest model is also a two-dimensional one applying only to a vertical plane or a case of a very wide channel. Recently, a very comprehensive water and sediment routing model based on

the depth averaging approach has been developed by Simons et al. (1979). They verified the applicability of an analytic model, supplemented by empirical relations, for simulating water and sediment movement in a river system. This model uses a finite-difference numerical scheme.

Both of the previous approaches have been adopted in the present study to develop two different finite-element schemes. One uses a two-dimensional vertical domain; the other employs a two-dimensional depth-averaging solution. Detailed information on Mathematical Formulation, Numerical Modeling and Solution, and Simulation Results are presented in Parts 2, 3, and 4, respectively. A complete computer program listing is given in the addendum 2.

2 FORMULATION OF MATHEMATICAL MODEL

2.1 EQUATIONS OF WATER MOVEMENT

In order to make mathematical modeling a possibility, many basic assumptions and simplifications are necessary. Since there is no theory which can include the fluid flow and moving boundary of the sediment particles 'simultaneously', the flow in an alluvial channel is to be broken into two physical phenomena and studied in a alternating sequence. That is, the hydrodynamic characteristics of a fluid flowing along a channel with an "instantaneously fixed" sand bed of a given geometry are studied first, and then the deformation of the sand bed is calculated using local sediment discharge determined from the hydrodynamic characteristics as well as from the sediment properties. The time-dependent phenomena of fluid flow and bed deformation are simulated by carrying out these two steps of solution procedure repeatedly.

In developing the mathematical model to describe the flow of water along a channel with "instantaneously fixed" sand bed boundaries, the conservation laws of mass and momentum for incompressible, viscous fluids are applied. Written in tensor form, they are:

$$v_{i,i} = 0, \quad i = 1, 2, 3, \quad (1)$$

$$\dot{v}_i + (v_i v_j)_{,j} + (p_{,i} - \tau_{ij,j})/\rho = F_i \quad i & j = 1, 2, 3, \quad (2)$$

Where v_i is the i th component of the velocity vector; p , ρ , and ν are pressure, density, and kinematic viscosity of the fluid, respectively;

τ_{ij} are components of the stress tensor which represent laminar or turbulent stresses; F_i is the i th component of the external (gravitational) body force per unit mass; $v_{,j}$ and \dot{v} represent partial derivatives of the function v with respect to the coordinate direction x_j and time, t , respectively. The summation convention is adopted for repeated indices throughout this work. For laminar flow, the expression for stress tensor is

$$\tau_{ij} = \mu(v_{i,j} + v_{j,i}) \quad (3)$$

In the case of turbulent flow, however, a different closure scheme is used to complete the mathematical model. It is beyond the scope of this study to review all existing schemes. Therefore, only those used in the present work will be discussed whenever they are introduced.

Boundary conditions needed for the fluid flow simulation are that (1) neither slip nor seepage are allowed at the channel boundaries, where the pressure is left to be determined by applying the governing equations at the boundary; (2) on the free surface the pressure is taken as constant; (3) the shear stresses acting on the free surface are neglected, which implies that the maximum velocity occurs at the free surface; (4) the flow is considered to be fully developed or uniform at the upstream end of the channel, and (5) appropriate boundary conditions are imposed at the downstream end. Also assumed is that the sand bed will be of uniform roughness and fixed instantaneously. And, although the sand bed has been assumed flat to start the simulations, any prescribed bed form (not necessarily flat) can be used as an initial condition without difficulty. More about bed deformation will be discussed later. Now, the attention is still centered on the mathematical modeling of the open channel flow with instantaneously fixed boundaries.

Although realistic mathematical models of flows in natural streams should be both three-dimensional and time-dependent, the computer storage capacity required to store the information and the computing time needed to obtain converged solution is too expensive to justify its use for a preliminary analysis of basic characteristics of flows in an alluvial channel. Therefore, a more practical alternative is needed. As mentioned above, two viable alternatives discussed in this report are used to treat horizontal shallow flows, and vertical flows with negligible variations in the lateral direction. These two approaches are presented below.

a. Depth-Averaging Model: This approach has been found to be both adequate and efficient for shallow water flows in which the variation of the hydrodynamic characteristics is predominantly horizontal. That is, velocity variations in the horizontal plane are greater than variations in the vertical, and the pressure distribution along the vertical axis may be assumed to be hydrostatic. In such cases, an efficient as well as adequate approximation to the three-dimensional flow problem is to treat the vertically averaged flow properties in a horizontal plane. To derive the model, let us, first, represent the bed and free surface geometries by $\zeta(x,y,t)$ and $\eta(x,y,t)$ respectively as shown in Fig. 1.

Although both the channel bed and free surface of the flow are, in general, deformable in time, for the convenience of numerical solution, they are assumed frozen instantaneously during the solution of flow properties. But, when the flowfield is solved, the elevations of both channel bed $\zeta(x,y,t)$ and free surface of the flow $\eta(x,y,t)$ are replaced by their new values before the flowfield is solved again for the next time step. The method to obtain new values of ζ and η will be given later when the technique for estimating sediment discharges is described.

The boundary conditions described in the previous section can then be translated into the mathematical equations. On the instantaneously frozen channel bed, $z = \zeta(x,y)$, they are:

$$v_i = 0, i = 1, 2 \text{ and } 3 \quad (4)$$

and at the free surface, $z = \eta(x,y,t)$, they are:

$$p = p_0 \quad (5)$$

$$\dot{\eta} + v_j \eta_{,j} = v_3, \quad j = 1 \text{ and } 2 \quad (6)$$

$$\tau_{i3} - \tau_{ij} \eta_{,j} = \tau_i^s, \quad i \text{ and } j = 1 \text{ and } 2 \quad (7)$$

Where p_0 is the atmospheric pressure and τ_i^s is the i th component of the surface (wind) shear stress. A similar expression may be written for the bed shear stress, τ_i^b . Integrating Eqs. 1 and 2 and using U and V to represent the vertically averaged properties of v_1 and v_2 respectively, one can get

$$\begin{aligned} \frac{\partial(hU)}{\partial t} + \frac{\partial(hU^2)}{\partial x} + \frac{\partial(hUV)}{\partial y} + gh \frac{\partial\eta}{\partial x} - \frac{1}{\rho} \frac{\partial(hT_{xx})}{\partial x} - \frac{1}{\rho} \frac{\partial(hT_{xy})}{\partial y} \\ - \frac{1}{\rho} (\tau_x^s - \tau_x^b) = 0 \end{aligned} \quad (8)$$

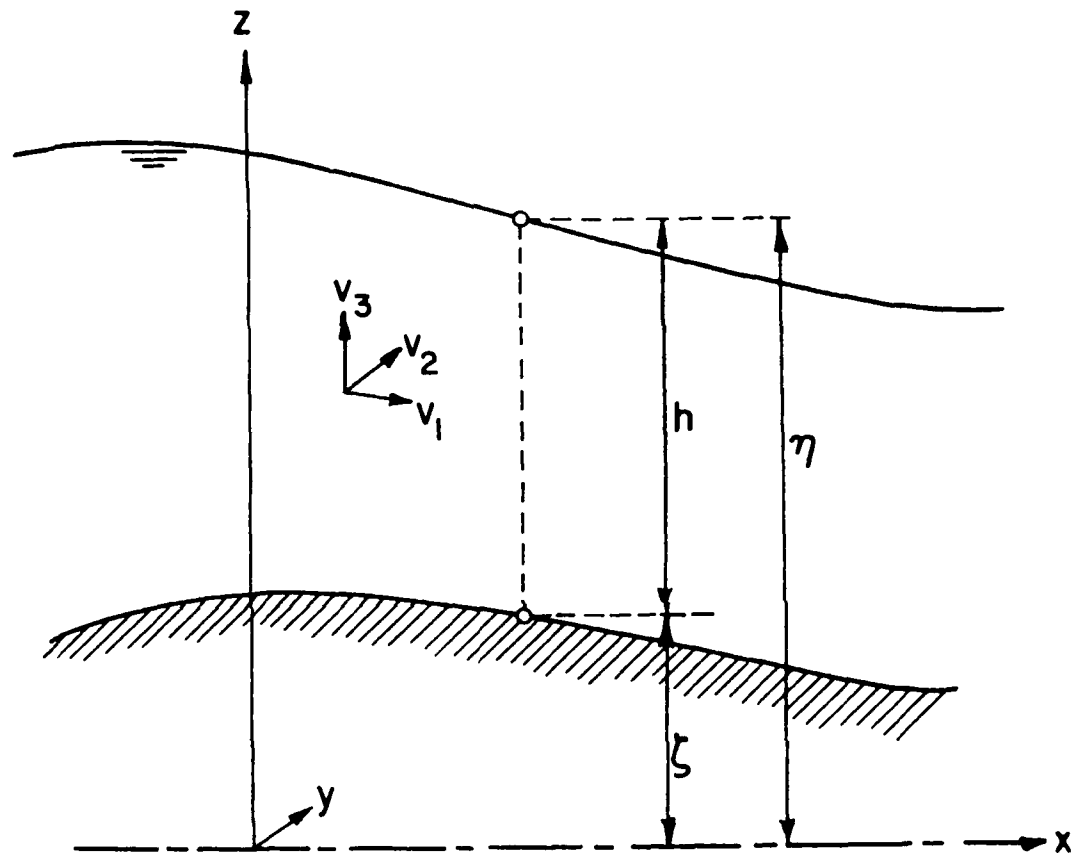


Fig. 1. The Coordinate System

$$\frac{\partial(hV)}{\partial t} + \frac{\partial(hUV)}{\partial x} + \frac{\partial(hV^2)}{\partial y} + gh \frac{\partial \eta}{\partial y} - \frac{1}{\rho} \frac{\partial(hT_{yx})}{\partial x} - \frac{1}{\rho} \frac{\partial(hT_{yy})}{\partial y} - \frac{1}{\rho} (\tau_y^s - \tau_y^b) = 0 \quad (9)$$

$$p = p_o + \rho g (\eta - z) \quad (10)$$

$$\frac{\partial h}{\partial t} + \frac{\partial(hU)}{\partial x} + \frac{\partial(hV)}{\partial y} = 0 \quad (11)$$

where g is the acceleration of gravity, and T_{ij} are effective stresses acting on vertical planes. During the integration, the Leibnitz rule, e.g.

$$\begin{aligned} \frac{\partial}{\partial t} \int_{\zeta}^{\eta} f(x, y, z, t) dz &= \int_{\zeta}^{\eta} \frac{\partial f}{\partial t} dz \\ &+ f(x, y, \eta, t) \frac{\partial \eta}{\partial t} - f(x, y, \zeta, t) \frac{\partial \zeta}{\partial t} \end{aligned} \quad (12)$$

and the boundary conditions (6) and (7) have been applied.

The bed shear stresses are assumed to have the same magnitude as those in steady uniform flow, and their directions to be the same as those of the depth-averaged velocity components. Their mathematical representations are

$$(\tau_x^b; \tau_y^b) = \rho f(U^2 + V^2)^{1/2} (U; V) \quad (13)$$

where f is a dimensionless friction factor defined in terms of either the Chezy coefficient, C_f , or the Manning's roughness coefficient, n , as given below:

$$f = g C_f^{-2} \text{ or } f = g n^2 (1.49)^{-2} h^{-1/3} \quad (14)$$

To enable the model to simulate eddies and circulations in the depth-averaged two-dimensional flow, the effective-stress terms have been taken into account. By analogy with the eddy-viscosity approach used in some turbulence closure schemes, an eddy-viscosity, ε , is introduced, so that the effective-stress terms in Eqs. 8 and 9 are replaced by

$$-\varepsilon h \left(\frac{\partial^2 U}{\partial x^2} + \frac{\partial^2 U}{\partial y^2} \right) \quad (15)$$

and,

$$-\varepsilon h \left(\frac{\partial^2 V}{\partial x^2} + \frac{\partial^2 V}{\partial y^2} \right) \quad (16)$$

respectively. As a first approximation, the coefficient of eddy viscosity can be related to the mean flow properties by

$$\varepsilon = Eh (U^2 + V^2)^{1/2} \quad (17)$$

where E is an adjustable eddy-viscosity parameter. Thus, the derivation of the depth-averaging model has been completed.

b. Two-Dimensional Vertical Flow Model: In this case lateral changes in flow and bed material properties are neglected. In tracking the bed-profile evolution, advantage is taken of the fact that the bed deforms at a rate much slower than the rate of change of free-surface transients. The water discharge hydrograph is replaced by a piecewise continuous distribution with time increments smaller than the time scale of the bed transients. During these time increments the water surface profile is computed by assuming a one-dimensional spatially varied steady flow. This permits the uncoupling of the bed profile calculations from the water routing scheme. Thus, the flow governing equations are the well known spatially varied flow equations

$$\bar{u} \bar{u}_{,x} + g h_{,x} + g z_{b,x} + g \bar{u} \bar{u} / C_f^2 h = 0 \quad (18)$$

and

$$\bar{u} h = q \quad (19)$$

where \bar{u} is the depth-averaged velocity, h is the flow depth, z_b is the bed elevation, x is the streamwise distance, g is the acceleration of gravity, C_f is the Chézy friction coefficient, and q is the water discharge per unit width. Within the context of the one-dimensional flow assumption, the flow geometry is restricted to situations where no separation occurs and where nearly parallel flow conditions exist. Under these conditions the vertical velocity distribution at any section is assumed to follow the logarithmic law

$$u = \frac{u_*}{k} \ln \frac{30(z-z_b)}{k_s} \quad (20)$$

in which u_\star is the local bed shear velocity; κ is the von Karman constant, k_s is the equivalent grain roughness, and z denotes the vertical position. Integrating Eq. 20 over the flow depth gives

$$u_\star = \kappa \bar{u} \left\{ \ln(30 h/k_s) - 1 \right\}^{-1} \quad (21)$$

which permits the estimation of u_\star from known local flow parameters.

2.2 EQUATIONS OF SEDIMENT MOVEMENT

As discussed in the previous chapter, the sediment transport phenomenon associated with the flow in an alluvial channel is, unfortunately, too complex to be described completely by analytical techniques, because the theories for describing the bed load of sediment as well as the boundary condition of sediment concentration on the bed surface have not yet been developed. The several practical sediment transport models that have been adopted most often can be classified into three categories:

1. By assuming that the sediment is being transported predominantly in suspension, the bed load is included in the suspended load and the sediment diffusion-convection equation can be solved for the sediment concentration distribution by analytical or numerical schemes. Then, the sediment discharge is computed by integrating the mass flux over a cross-section area normal to the flow direction. The drawbacks of this approach are: first, the boundary condition for sediment concentration on the surface of the channel bed is still not understood completely. Secondly, the estimation of sediment discharge may not have sufficient accuracy for the cases in which the bed load can no longer be neglected.

2. The sediment discharge is estimated by combining the suspended discharge and the bed discharge. The suspended discharge is solved analytically using the approach similar to that described above in the category 1. The bed discharge is, however, estimated using one of the empirical functions which have been developed in recent years. A good review concerning the capabilities and limitations on those bed load formulas may be found in Graf (1971). The major drawbacks of these kind of approaches are that, first, they are more involved than the first category approach, and second, it is difficult to find an accurate formula for determining the concentration boundary condition near the surface of the channel bed. This latter drawback has to be resolved, before this approach can be widely adopted.

3. Without distinguishing the suspended and bed load, one may select one appropriate empirical formula to compute the total sediment transport load. The obvious advantage is the simplicity of this approach when it is used to simulate a particular section of a particular alluvial channel. However, a different formula may have to be adopted for a different channel or even a different section of the same channel. This drawback can sometimes be alleviated by calibrating an adjustable parameter existing in the empirical function chosen for a particular channel, or even calibrating it from section to section of a channel, so that an accurate sediment transport model can be established.

Although all three different approaches have been used in the course of this research, the mathematical formulations of the first and the third approaches are described below, because they have produced some good results.

a. Depth-Averaging Model: In simulating depth-averaged flows predominantly in a horizontal plane the total sediment transport load is represented by an empirical formula. For example, a model based on a power function of the mean velocity may be used conveniently to estimate the total load with its coefficient and exponent being calibrated for individual cases. This model has been successfully adopted by other researchers (Simons et al., 1979, DeVries, 1973). Therefore, it is applied to perform a preliminary study on the deformation of sand bed due to sediment transport by the fluid.

The sediment transport function selected for the present study is of the form

$$g_i = c_g \rho V_i^m \quad (22)$$

where g_i is the bed material transport function in the direction of depth-averaged velocity component V_i , c_g and m are the coefficient and exponent respectively. For a particular channel geometry and bed material characteristics, c_g and m are estimated or calibrated using experimental information. After the depth-averaged flow field is solved, the sediment discharge can be easily computed.

Then, the bed material continuity equation

$$q_{s,x} + q_{s,y} + (1 - \lambda) z_{b,t} = 0 \quad (23)$$

is used to calculate a new bed elevation z_b . And, the complete physical system has, thus, been represented by a mathematical model. In this equation λ denotes the porosity of the bed material.

b. Two-Dimensional Vertical Flow Model: The preceding profile computations are based on the assumption that the local flow transport capacity does not deviate significantly from equilibrium conditions, and no distinction is made between bed and suspended transport mode. Such an approach is justified if either bed-load transport is predominant, or the sediment is being routed over long reaches. Otherwise, the assumption of near equilibrium capacity is not valid because the bed load reacts immediately to changes in local flow conditions while the suspended load tends to react more slowly. This slow adaptation of the suspended load can significantly influence the bed profile evolution over relatively short reaches (Kerssens et al., 1977); Fredsøe, 1978). For this reason, the present analysis includes the equation governing the dispersion of suspended sediment, in addition to the bed-material continuity equation. These equations are simplified by assuming that:

- i. Longitudinal dispersion can be neglected in relation to the vertical dispersion;
- ii. The sediment settling velocity, v_s , is invariant;
- iii. Vertical convection is negligible in a nearly horizontal flow;
- iv. The time rate of change of the sediment concentration is not significant (Mahmood, 1975);
- v. The bed material is fairly uniform in size, and can be represented by an effective particle diameter.

The sediment dispersion equation thus yields

$$u c_{,x} - v c_{,z} = (\varepsilon c_{,z})_{,z} \quad (24)$$

where c is the point volumetric concentration, and ε_z is the vertical sediment transfer coefficient. By averaging Eq. 24 over the flow depth the following bed-material continuity equation is obtained

$$q_{s,x} + (1-\lambda) z_{b,t} = 0 \quad (25)$$

in which q_s is the volumetric discharge of bed material per unit width, λ is the bed porosity, and t is time.

Since Eqs. 18, 19, 20, 24, and 25 describe an evolutionary process, appropriate initial and boundary conditions need to be specified. They are the initial bed profile, the upstream bed elevation and inflow of water and sediment, the downstream flow stage and streamwise concentration gradient, and vanishing sediment flux across the free surface. These conditions are represented by

$$z_b(x;0) = z_0(x), \quad 0 \leq x \leq L, \quad t = 0 \quad (26)$$

$$q(0;t) = g(t), \quad x = 0, \quad t \geq 0 \quad (27)$$

$$q_s(0;t) = r(t), \quad x = 0, \quad t \geq 0, \quad (28)$$

$$c(0,z;t) = s(z;t), \quad x = 0, \quad 0 \leq z - z_b \leq h, \quad t \geq 0 \quad (29)$$

$$z_b + h = H(t), \quad x = L, \quad t \geq 0, \quad (30)$$

$$c_{,x} = [(\varepsilon_z c_{,z}), z + v_s c_{,z}] / u, \quad x = L, \quad 0 \leq z - z_b \leq h, \quad t \geq 0, \quad (31)$$

$$v_s c + \varepsilon_z c_{,z} = 0, \quad 0 \leq x \leq L, \quad z = z_b + h, \quad t \geq 0. \quad (32)$$

In these equations, z_0 , g , r , s , and H are given continuous functions, H represents the downstream stage, and L is the length of the reach. The sediment concentration over the upstream boundary, condition 29, is determined by solving Eq. 24 for the equilibrium case ($c_{,x} = 0$) and by specifying an appropriate distribution for ε_z . From regression analysis of point measurements of the sediment transfer coefficient conducted by Coleman (1970), Kerssens et al. (1977) obtained the following expression for the transfer coefficient.

$$\varepsilon_z = \varepsilon_{\max} [4 \zeta (1-\zeta)]^\delta \quad (33)$$

where

$$\zeta = (z - z_b)/h,$$

$$\varepsilon_{\max} = u_* h [0.13 + 0.2 (v_s/u_*)^{2.12}]$$

$$\delta = 1, \quad 0 < \zeta \leq 0.5,$$

$$\delta = 0, \quad 0.5 < \zeta \leq 1.$$

Using this equation the following equilibrium concentration distribution results

$$c = h u_* c_a [\zeta_a / (1-\zeta_a)]^\beta \times [(1-\zeta)/\zeta]^{\beta\delta} \exp[2\beta(\delta-1)(2\zeta-1)], \quad (34)$$

in which

$$\beta = h v_s / 4 \varepsilon_{\max},$$

and c_a is the concentration at a point $\zeta_a > 0$ near the bed. An estimate of the reference value c_a is obtained by assuming that most of the sediment is carried in suspension, and then matching the sediment flux through the upstream section to a suitable total load formula. That is,

$$q_s = \int_{\zeta_a}^1 u c \cdot d\zeta \quad (35)$$

Kerssens et al. (1977) found the following modified version of the formula developed by Engelund and Hansen (1967) to agree well with their measured loads

$$q_s = 0.035 \bar{u}^5 / [d_{50} (S-1)^2 g^{1/2} C_f^3], \quad (36)$$

where q_s is the sediment volumetric discharge in $m^3/sec.m$, d_{50} is the bed material size in meters, and S is the sediment specific gravity. Substituting Eqs. 20, 34 and 36 into Eq. 35 yields

$$\frac{0.035 \bar{u}^5}{h u_* d_{50} (S-1)^2 g^{1/2} C_f^3} [(1 - \zeta_a)/\zeta_a]^\beta = \\ C_a \int_{\zeta_a}^1 \ln(30\zeta/k_s) [(\zeta - \zeta_a)/\zeta_a]^{\beta\delta} \exp [2\beta(\delta-1)(2\zeta-1)] d\zeta \quad (37)$$

from which C_a can be determined. The integral on the right side is evaluated using Gaussian quadrature.

NUMERICAL SOLUTIONS

3.1 DEPTH-AVERAGING MODEL

A typical finite element system used to discretize a continuous horizontal domain is shown in Fig. 2.

Isoparametric interpolation functions are used to relate the properties at any point within an element to those at nodal points of the same element. For linear cases, they are of the form:

$$(U; V; h) = \alpha_n (U_n; V_n; h_n) \quad (38)$$

$$\text{where: } \alpha_n = \frac{1}{3} (1 + \zeta_n \zeta) (1 + \eta_n \eta), \quad n = 1, 2, 3, \text{ and } 4 \quad (39)$$

The transformation between the global (x, y) and the local (ζ, η) coordinate systems is specified by

$$(X; Y) = \alpha_n (X_n; Y_n). \quad (40)$$

To reduce the degree of nonlinearity, the hydraulic depth, h , in the momentum equations at all nodes are estimated initially and corrected during the iterative solution procedure. Due to the fact that the bed deforms at a rate much slower than the rate of change in hydrodynamic properties, the hydrodynamic equations and the bed form model are decoupled. And, since the bed form can be considered being instantaneously fixed during the solution of hydrodynamic equations, the assumption of quasi-steady flow should give satisfactory solution. Therefore, the fluid flow equations are simplified into the following form:

$$U \frac{\partial U}{\partial X} + V \frac{\partial U}{\partial Y} - \epsilon (\frac{\partial^2 U}{\partial X^2} + \frac{\partial^2 U}{\partial Y^2}) + \frac{g w^*}{C_f^2 h^*} U + g \frac{\partial \eta}{\partial X} = 0 \quad (41)$$

$$U \frac{\partial V}{\partial X} + V \frac{\partial V}{\partial Y} - \epsilon (\frac{\partial^2 V}{\partial X^2} + \frac{\partial^2 V}{\partial Y^2}) + \frac{g w^*}{C_f^2 h^*} V + g \frac{\partial \eta}{\partial Y} = 0 \quad (42)$$

$$h \frac{\partial U}{\partial X} + h \frac{\partial V}{\partial Y} + U \frac{\partial h}{\partial X} + V \frac{\partial h}{\partial Y} = 0 \quad (43)$$

$$\text{where } w^* = (U^{*2} + V^{*2})^{\frac{1}{2}}$$

Applying the Method of Weighted Residual (MWR) after Galerkin, the finite element equations for each and every element are formulated.

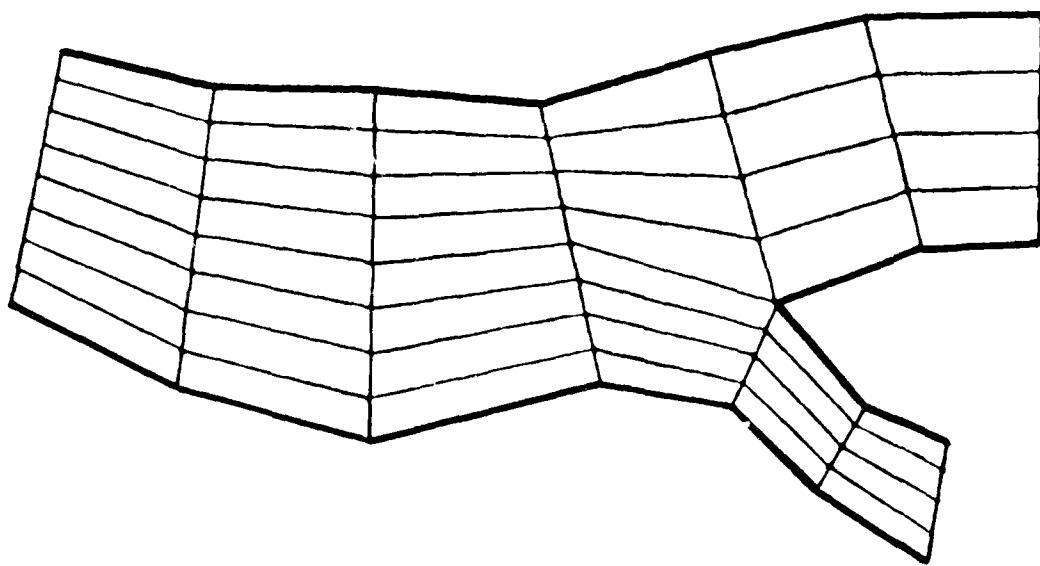


Fig. 2. A typical finite element grid using quadrilateral elements

$$A_{n\ell m} U_{\ell} U_m + B_{n\ell m} V_{\ell} U_m + C_{nm} U_m + D_{nm} U_m + E_{nm} h_m - H_n = 0 \quad (44)$$

$$A_{n\ell m} U_{\ell} V_m + B_{n\ell m} V_{\ell} V_m + C_{nm} V_m + D_{nm} V_m + F_{nm} h_m - G_n = 0 \quad (45)$$

$$A_{n\ell m} h_{\ell} U_m + B_{n\ell m} h_{\ell} V_m + A_{n\ell m} U_{\ell} h_m + B_{n\ell m} V_{\ell} h_m = 0 \quad (46)$$

where $A_{n\ell m} = \int_A \alpha_n \alpha_{\ell} \alpha_m, x dA$

$$B_{n\ell m} = \int_A \alpha_n \alpha_{\ell} \alpha_m, y dA$$

$$C_{nm} = \int_A \varepsilon (\alpha_n, x \alpha_m, x + \alpha_n, y \alpha_m, y) dA$$

$$D_{nm} = \frac{g w^*}{C_f^2 h^*} \int_A \alpha_n \alpha_m dA$$

$$E_{nm} = g \int_A \alpha_n \alpha_m, x dA$$

$$F_{nm} = g \int_A \alpha_n \alpha_m, y dA$$

$$H_n = \int_{\ell} \varepsilon \bar{\alpha}_n (U_{,x} n_x + U_{,y} n_y) d\ell - g \frac{\partial \zeta}{\partial x} \int_A \alpha_n dA$$

$$G_n = \int_{\ell} \varepsilon \bar{\alpha}_n (V_{,x} n_x + V_{,y} n_y) d\ell - g \frac{\partial \zeta}{\partial y} \int_A \alpha_n dA$$

All sets of finite element equations, one set for each element, are assembled into the following global set. The actual assembling process is carried out by a computer program simultaneously with the evaluation of the coefficients of local element equations.

$$I_1 = A_{ijk} U_j U_k + B_{ijk} V_j U_k + \bar{C}_{ik} U_k + E_{ij} h_j - H_i \quad (47)$$

$$I_2 = A_{ijk} U_j V_k + B_{ijk} V_j V_k + \bar{C}_{ik} V_k + F_{ij} h_j - G_i \quad (48)$$

$$I_3 = A_{ijk} h_j U_k + B_{ijk} h_j V_k + A_{ijk} U_j h_k + B_{ijk} V_j h_k \quad (49)$$

This global set is solved iteratively by the Newton-Raphson technique to yield the flow field properties.

Then the sediment transport function, Eq. 22, is used to estimate the bed material discharge at each node. The sediment continuity equation is

discretized by the FEM, using the same element system, and interpolation functions. The resulting global equations are:

$$L_{ij} \Delta Z_j = K_i. \quad (50)$$

Substituting the sediment discharge results into this equation the new bed elevations at every node are obtained. Thus, the discretization of the mathematical model of the sediment transport phenomenon has been completed.

3.2 TWO-DIMENSIONAL VERTICAL FLOW MODEL

The Galerkin integral approximation within the Method of Weighted Residuals is used to derive the finite element equations. The first step of the solution involves dividng the continuous solution domain, Ω , into a set of nonoverlapping subdomains, Ω_e , or finite elements, such that

$$\Omega \cup \Gamma = \bigcup_{e=1}^E \Omega_e$$

where Γ is the boundary of the solution domain, and E denotes the total number of elements. The one-dimensional domain of Eq. 18 is discretized as shown in Fig. 3(a). In Fig. 3(b) the two-dimensional domain of Eq. 24 is divided into a series of isoparametric elements. The finite element grid is designed so as to provide greater resolution near the stream bed where high velocity and concentration gradients exist. Within each subdomain the unknown variables are interpolated in terms of their nodal values as

$$f_e(\vec{x};t) = \phi_n(\vec{x}) F_n(t), \quad \vec{x} \in \Omega_e, \quad (51)$$

where f_e stands for the interpolated values of all variables, F_n denotes values at a node n , and ϕ_n represents the interpolating functions. This study uses linear isoparametric functions, which have the advantage of satisfying the basic convergence criteria of completeness and continuity, and serve at the same time as coordinate transformation equations. For instance, for the two-dimensional elements

$$\phi_n = \frac{1}{4} (1+\zeta_n \xi)(1+\eta_n \eta) \quad (52)$$

where the isoparametric coordinates are related to the global coordinates such that the corner point (x_i , z_i , $i = 1, 2, 3, 4$) of a quadrilateral element are transformed into the four points (1,1), (1,-1), (-1,-1), (-1,1) in the (ξ, η) space. The approximate solutions are of the form

$$\hat{f}(\vec{x};t) = \bigcup_{e=1}^E f_e = \phi_n F_n, \quad \vec{x} \in \Omega, \quad (53)$$

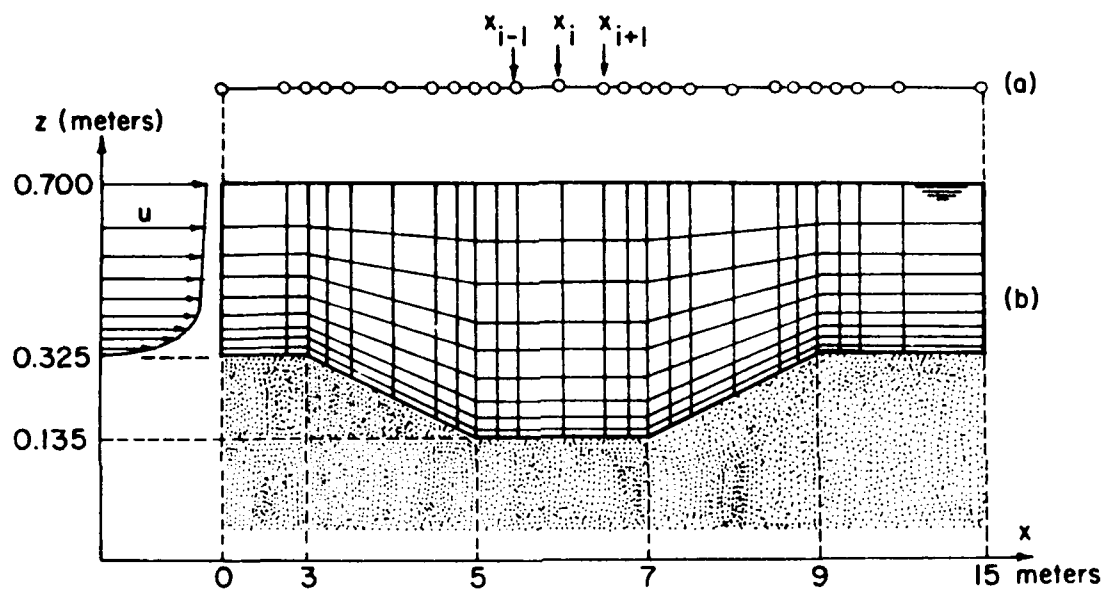


Figure 3. Sketch of finite element grid at $t = 0$

in which ϕ_n are linear functions of the spatial domain. When the solutions \hat{f} are substituted into the Eqs. 18, 19, and 24 approximation errors, or residuals, are introduced. The expansion coefficients F_n are determined by rendering these residuals orthogonal to the respective interpolation functions. This yields

$$\int_{\Omega_e} [g - q^2/h^3] h_{,x} + g(z_b, x + q^2/C_f^2 h^3)] \phi_n d\Omega_e = 0 \quad (54)$$

$$\iint_{\Omega_e} [\epsilon_{c,x} - (\epsilon_s + \epsilon_z z) c_{,z} - \epsilon_z c_{,zz}] \phi_n d\Omega_e = 0 \quad (55)$$

The integrand in Eq. 54 results from combining equations 18 and 19. After substituting the interpolation functions, applying the Green-Gauss theorem to the last term in Eq. 55, or integrating by parts, the preceding equations yield

$$L_{nm} H_m = M_n, \quad (56)$$

$$P_{n\ell m} U_\ell C_m + Q_{nm} C_m = R_n, \quad (57)$$

where $\ell, m, n = 1, 2, \dots, n_e$ (n_e = total number of element nodes), and

$$L_{nm} = \int_{\Omega_e} (g - q^2/\bar{h}^3) \phi_n \phi_m, x d\Omega_e, \quad (58a)$$

$$M_n = - \int_{\Omega_e} g(z_b, x + q^2/C_f^2 \bar{h}^3) \phi_n d\Omega_e, \quad (58b)$$

$$P_{n\ell m} = \iint_{\Omega_e} \phi_n \phi_\ell \sigma_{m,x} d\Omega_e, \quad (58c)$$

$$Q_{nm} = \iint_{\Omega_e} \epsilon_z (\phi_{n,z} \phi_{m,z} - \epsilon_{z,z} \phi_n \phi_{mmz}) d\Omega_e \quad (58d)$$

$$R_n = \int_{\Gamma_e} \epsilon_{z,z} (\bar{c}_{,z} \phi_n) \hat{n}_z d\Gamma_e. \quad (58e)$$

Here \hat{n}_z is the z-component of the unit vector normal to the element boundary Γ_e , and \bar{h} , \bar{c} represent either initial or iterated values. The coefficients (58) are evaluated in the (ξ, η) space. Since all elements are identical in this coordinate system, once the formulas for those coefficients are developed for one element the same formula is used for all the other elements. Eq. (58c) yields, for instance,

$$\begin{aligned}
 P_{n\ell m} &= \iint_{\Omega_e} \phi_n \phi_\ell \phi_m, x d\Omega_e \\
 &= \iint_{-1}^{+1} \phi_n \phi_\ell (\phi_m, \zeta \bar{J}_{11} + \phi_m, \eta \bar{J}_{12}) [J] d\zeta d\eta
 \end{aligned} \tag{59}$$

in which $[J]$ is the determinant of the transformation Jacobian, and J_{ij} are elements of the inverse Jacobian. In all cases the integrals are evaluated using a Gaussian quadrature subroutine.

Once evaluated, the coefficients of equations 56 and 57 are assembled into the corresponding global matrices. After introducing the Dirichlet-type boundary conditions, the global equations reduce to

$$L_{k\ell} H_\ell = M_k, \tag{60}$$

$$T_{k\ell} C_\ell = R_k, \tag{61}$$

where $T_{k\ell} = P_{k\ell m} U_\ell + Q_{km}$, and $k, \ell = 1, 2, \dots, N$. Here N is the total number of node points containing unknown values. The nonlinear equations 60 and 61 are solved iteratively using a subroutine developed for banded matrices. After the global nodal values H_ℓ are determined, Eq. 19 is used to obtain the corresponding velocities U_ℓ .

For convenience, the sediment continuity Equation 25 is discretized using the following explicit finite-difference scheme:

$$z_b^{i,j+1} = z_b^{i,j} - \frac{\Delta t}{(1-\lambda)} \frac{q_s^{i+1,j} - q_s^{i-1,j}}{x_{i+1} - x_{i-1}}, \tag{62}$$

where x_{i+1} and x_{i-1} are defined in Figure 1(a), and $\Delta t = t_{j+1} - t_j$ is the time increment. Equations 60 through 62 constitute the numerical algorithm used in the present case.

PRESENTATION AND EXAMINATION OF RESULTS

4.1 FLOW AROUND A SPUR DIKE IN A STRAIGHT CHANNEL WITH A SAND BED

A thin spur dike is placed in a straight alluvial channel with dimensions shown in Fig. 4. The variation of the flow field hydrodynamic behavior due to bed form changes in time is simulated using the depth-averaging model developed in the present study. The boundary as well as initial conditions used in this case are no slip on the solid walls, almost uniform flow at the entrance, parallel flow are left to be determined by the governing differential equations at the exit, no shear on the free surface of the water, bed material particles having uniform properties, and the bed being flat when the flow simulation is started. The computer simulated bed form and velocity distribution in the flow field after 5, 10, and 15 hours are shown in Figs. 5 through 10 for an average velocity = 0.110 ft/sec; water depth = 0.38 ft; channel width = 6 ft; dike opening = 4 ft; and the time step for sediment routing was $t = 3000$ sec. The velocity of flow accelerates locally increasing the carrying capacity, which can be seen in the area around the nose of dike in Figs. 7 and 10. When the flow decelerates downstream from the dike and loses carrying capacity, the deposition of sediment occurred. At the downstream end, the flow recovers equilibrium, and the carrying capacity is equivalent to the amount of sediment deposition. Therefore, the bed form essentially does not change. This test is a simulation of the bed scour around a spur dike measured by Zaghloul and McCorquodale (1975). They reported the geometry of the scour-hole developed around a dike mounted perpendicular to the flow direction in a laboratory flume with a movable bed. The maximum scour depth was observed right at the nose of the spur dike. The scour hole upstream of the dike was conical in shape, whereas downstream was elongated and had a shallower slope. No sediment deposition was reported. However, similar measurements conducted by Ahmad (1953) and by Garde et al. (1961) have shown that a deposition bar is formed adjacent to the spur dike on the downstream side. The simulated depth-average flow pattern and bed geometry obtained after 15 (real time) hours exhibit qualitative agreement with the shapes of the measured hole. However, the locations of the deepest point and deposition bar are incorrect. The reason is twofold: (i) the model does not reproduce the flow separation created by the stagnation region upstream of the dike. The result is an excessive flow component parallel

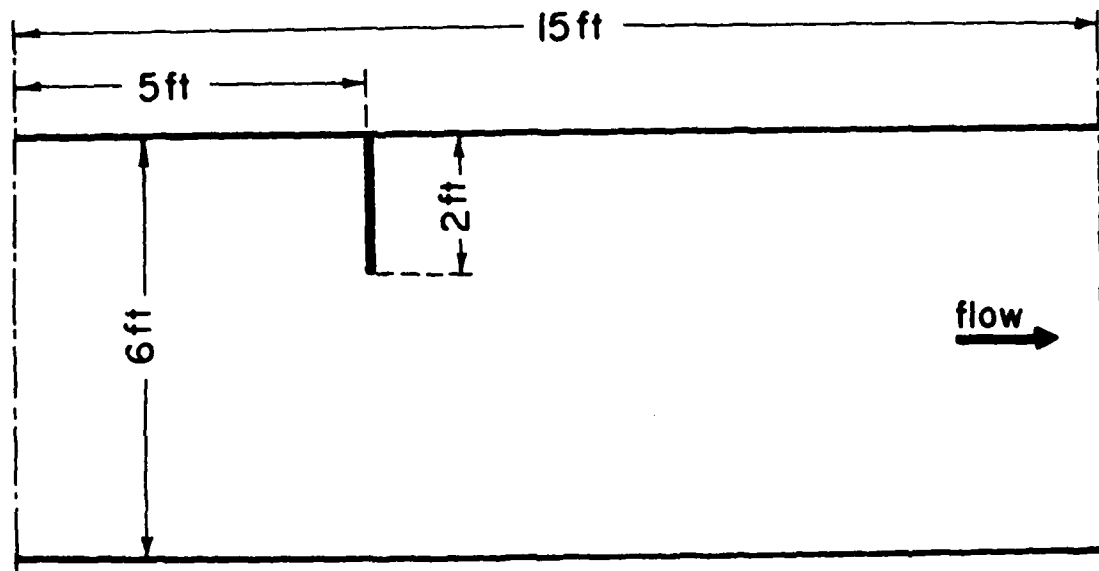


Fig. 4 Dimensions of Straight Channel with Spur Dike

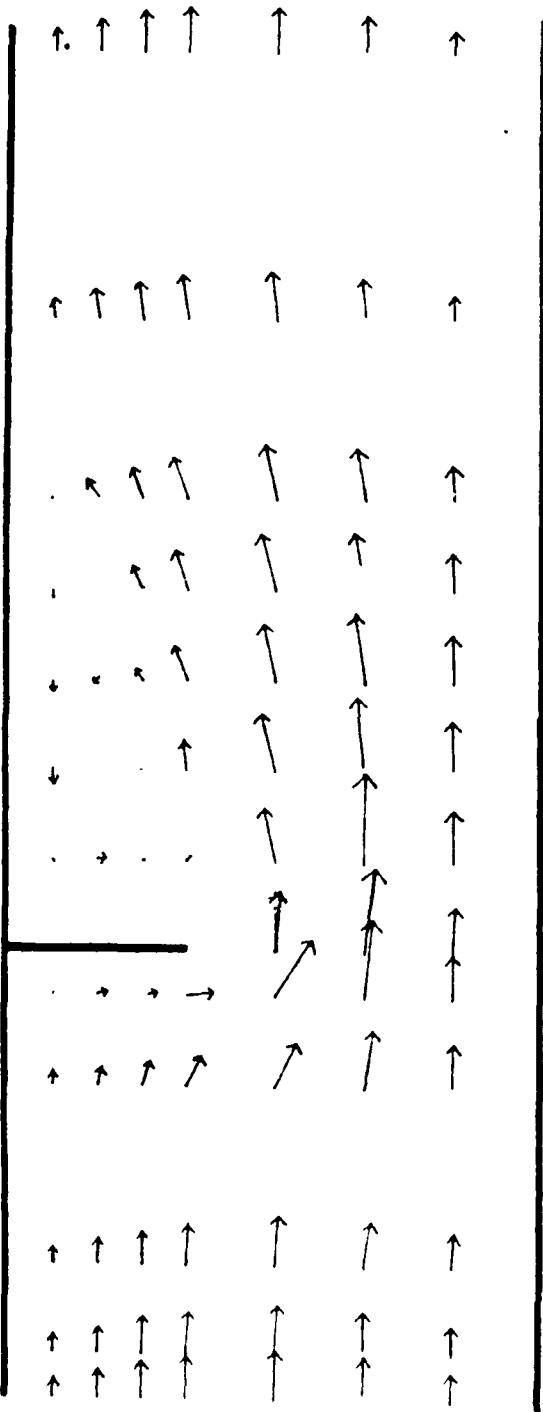


Fig. 5 Velocity distribution around spur dike after 5 hours.

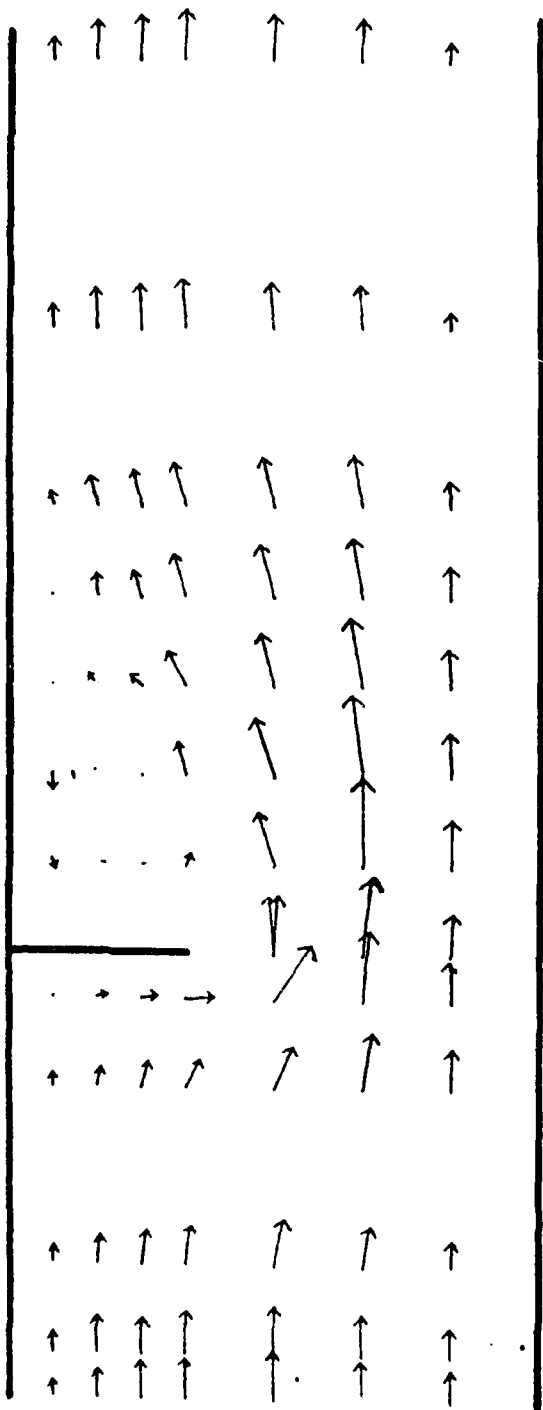


Figure 6. Velocity distribution around spur dike after 10 hours.

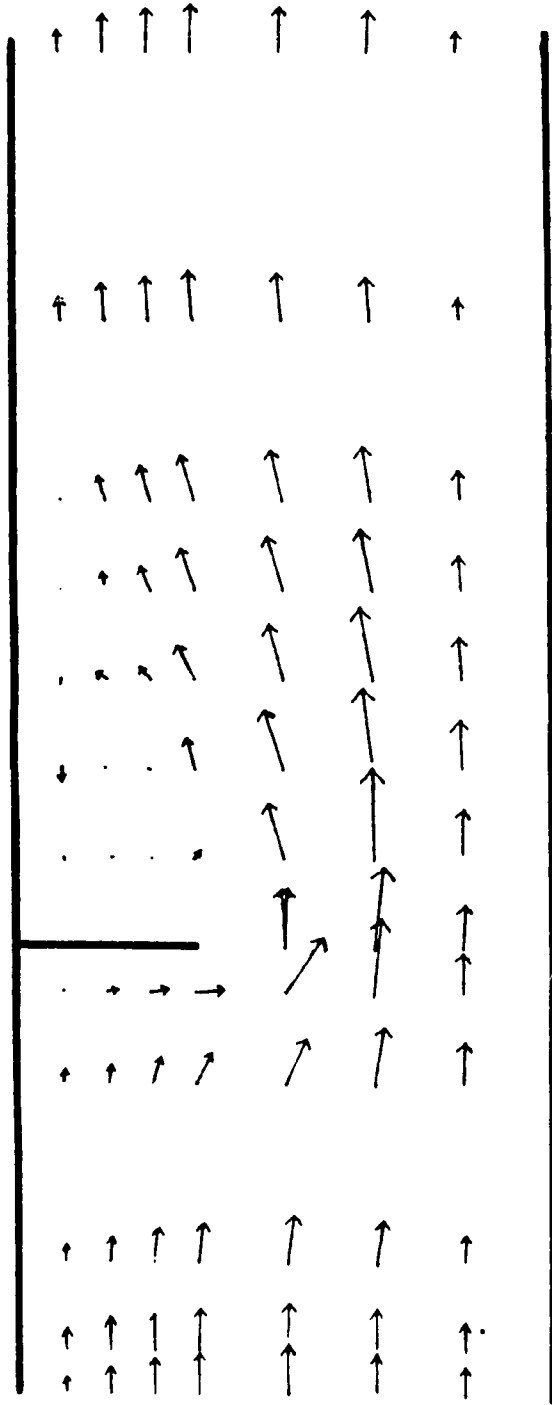


Fig. 7. Velocity distribution around spur dike after 15 hours.

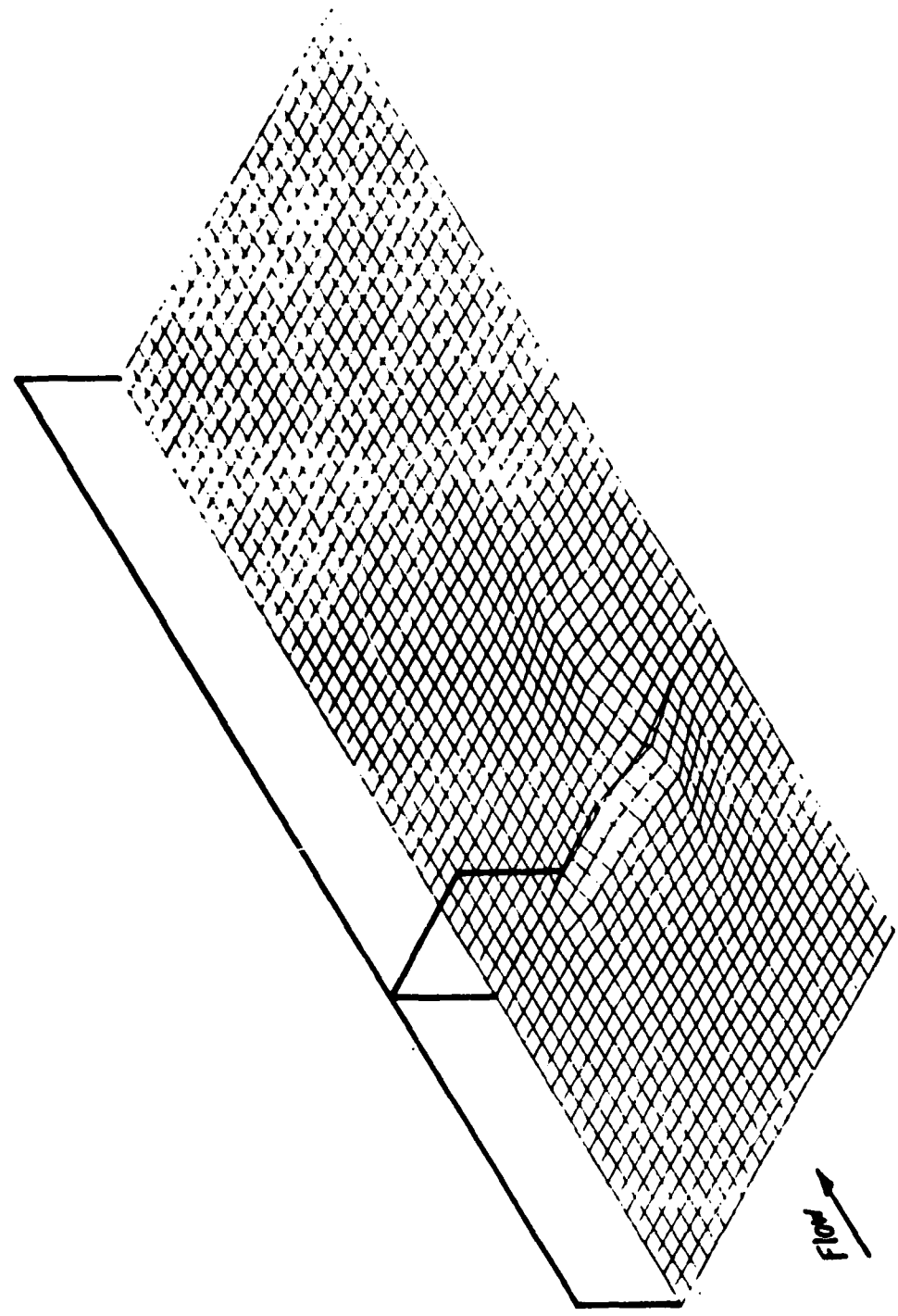


Figure 8. Bed deformation around spur dike after 5 hours.

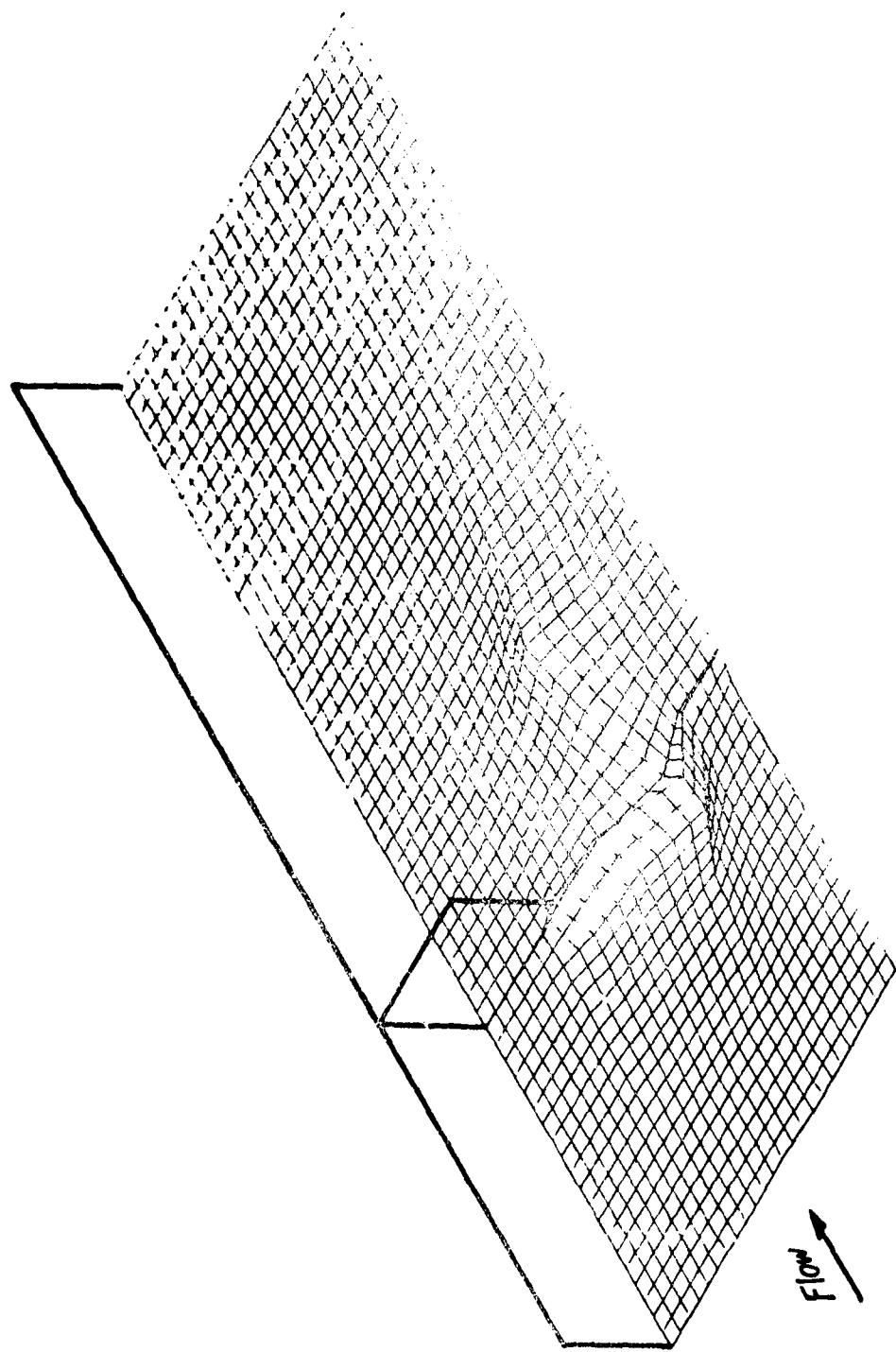


Fig. 9. Bed deformation around spur dike after 10 hours.

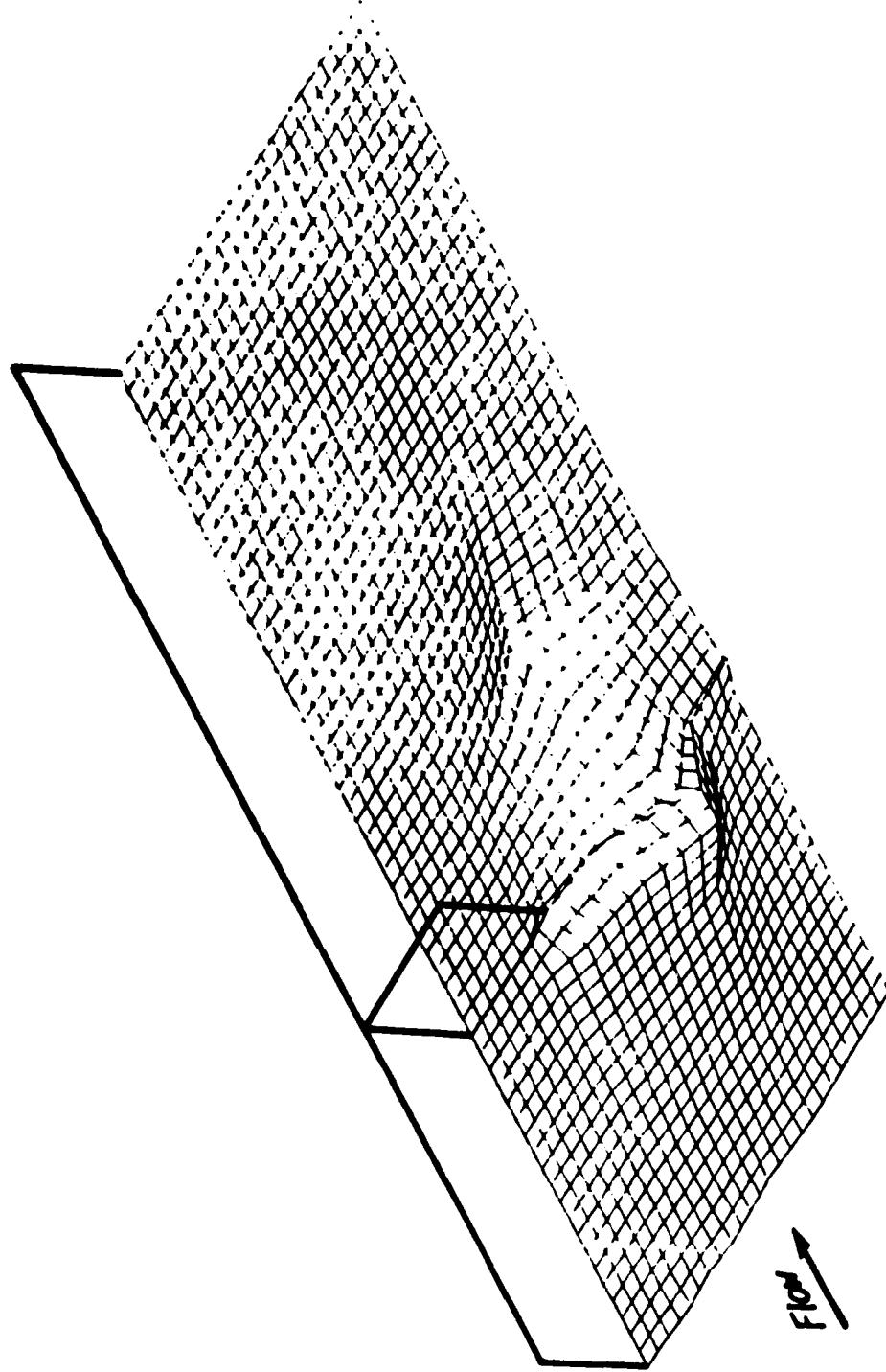


Fig. 10. Bed deformation around spur dike after 15 hours.

to the dike that forces the region of maximum velocity away from the dike-nose; (ii) the low velocities predicted along the shear layer emanating from the dike induce a backflow circulation that is too weak to transport bed-load material from the primary stream to the downstream side of the dike. The results point out a deficiency in the model when simulating situations dominated by regions of flow separation. Further research is needed to correct this deficiency. The CPU time required for this simulation was ten minutes per each hour of real time.

4.2 LOCAL SCOUR AND FILL OF A TRENCH IN A SAND BED STREAM

The natural backfilling of a trench dredged across an alluvial streambed is also studied using the two-dimensional model in a vertical plane. This simplification is valid provided that both the stream and the trench are wide enough to neglect the variation of properties in the lateral direction of the flow. The computer program developed for this simulation is basically similar to the depth-averaged model in a horizontal plane, so that it is not necessary to present it here.

The schematics of the finite element system and initial bed form and flow conditions are shown in Fig. 3. The dynamic behavior of the finite element system is clearly seen from Fig. 11, which represents the condition of the flow and deformed sand bed as well as free surface at a later time ($t > 0$). The coordinate, or position, of each node is adjusted at each time step whenever the bed and/or surface elevation change during the time interval. By doing this the computing scheme is more stable and efficient than the one with fixed interior nodes and moving boundary nodes.

The computer simulated bed and free surface profiles at 7 and 14 hours after the numerical experiment is turned on are shown in Fig. 12. It is very obvious that the computer simulation can indeed produce reasonable results, which are verified by data obtained from physical experiment. This case was studied for the purpose of verification with a set of data collected at the de Voorst Hydraulic Laboratory, The Netherlands, by Kerssens, et al. (1977). In that experiment, a trench having the geometry shown in Fig. 3 was formed in a 0.127 mm sand bed in a laboratory flume. Water was circulated over the bed at a steady rate of $0.195 \text{ m}^3/\text{sec}\cdot\text{m}$, while the downstream stage was maintained at a constant level. Sediment was supplied at a constant rate of $0.041 \text{ kg/sec}\cdot\text{m}$, and most of the load was carried in suspension. Due to hydraulic sorting the d_{50} of the suspended

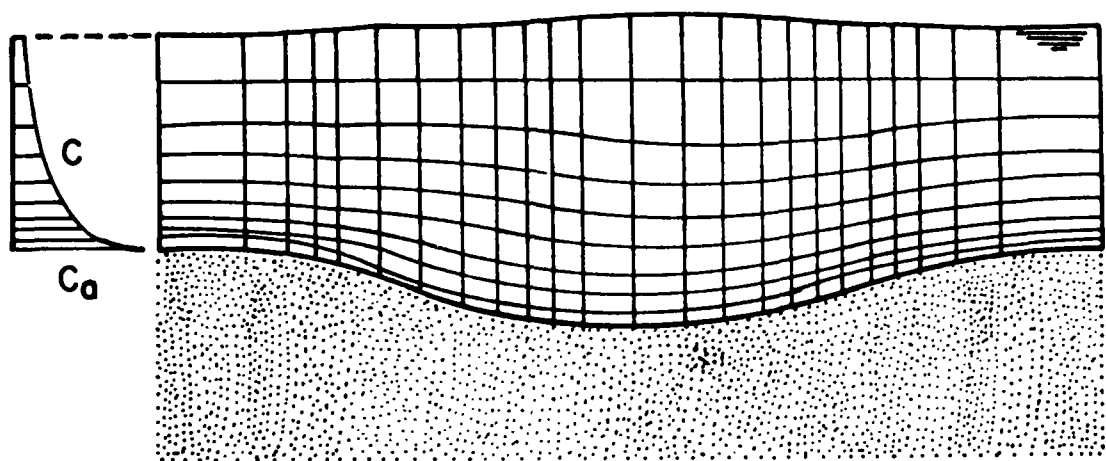


Fig. 11. Sketch of finite element grid at $t > 0$.

bed material approached a value of 0.110 mm with a settling velocity of 0.01m/sec. During the run ripples formed on the bed and the Nikuradse sand roughness was estimated at 0.025 m. The Chezy friction coefficient, corrected for side-wall effects, was about $36 \text{ m}^2/\text{sec}$ on the reach upstream of the trench.

The bed profile was measured after 7 and 14 hours of continuous flow. These profiles are shown in Figure 15 along with the simulated free-surface and bed elevations. A reference concentration level equal to 0.015 m, or slightly over half the ripple height, was used in the simulation. The comparison between the observed and simulated bed profiles is satisfactory. The largest shape discrepancy occurs on the converging sideslope of the trench. This may have been caused by the failure of the assumed velocity profiles to account for the increase in velocity gradients near the bed induced by the flow acceleration. The water-surface profiles correctly reproduce the surface rise over the trench. As the trench is filled up the water crest diminishes and moves downstream with the trench, as expected.

Fig. 13 depicts the distribution of suspended sediment throughout the flow domain after 7 hours. The contours of constant concentration were drawn from computed results. This plot illustrates the deposition of sediment occurring on the downstream side of the trench as the stream decelerates and loses carrying capacity. As the flow regains velocity, sediment is entrained along the upstream side and diffused upwards. The suspended material leaving the trench area gradually approaches a new equilibrium distribution. The CPU time was approximately four minutes per hour of real time. The computer memory required by the codes used in the tests presented above was 100,000 words.

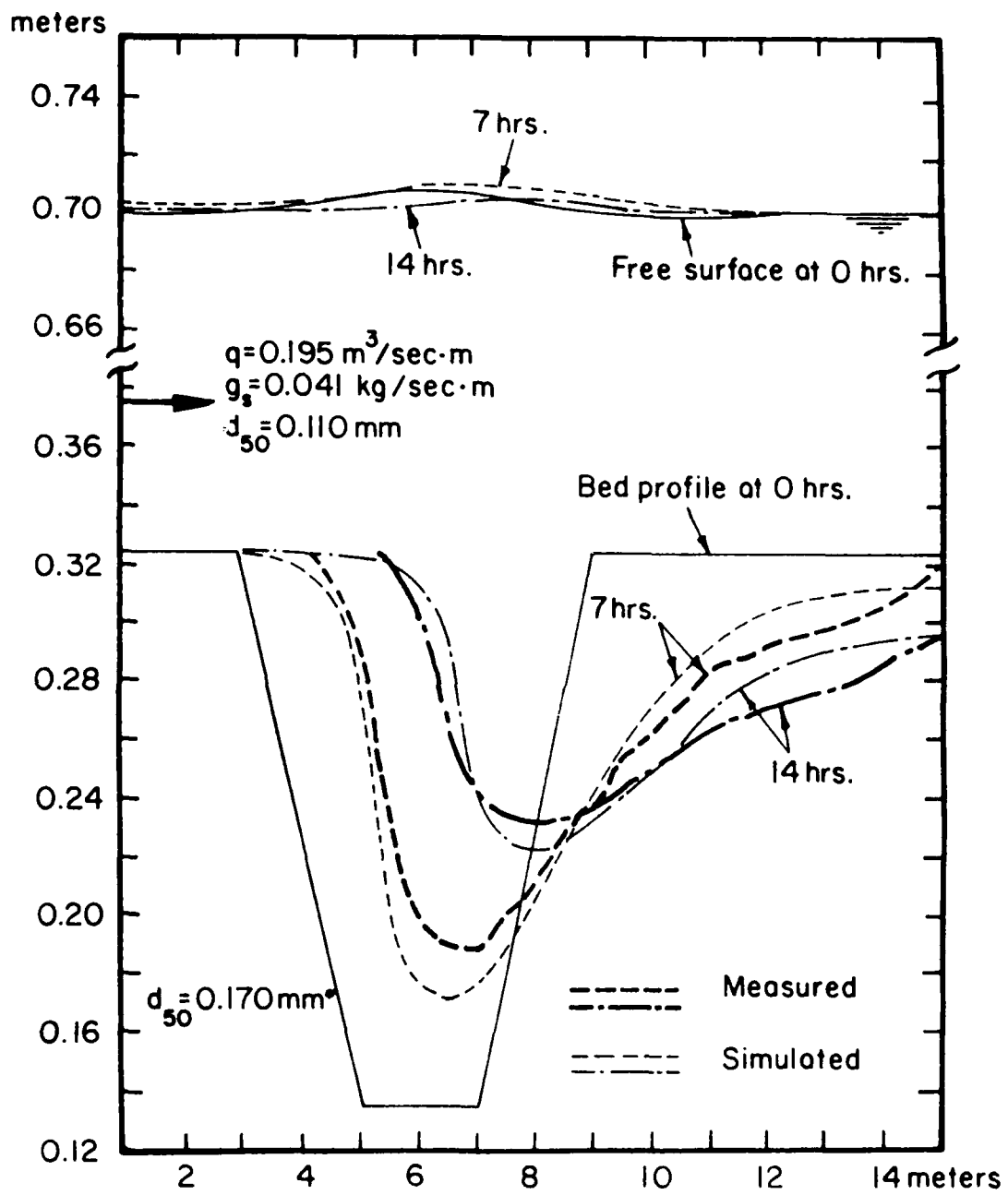


Fig. 12. Evolution of free-surface and bed profiles.

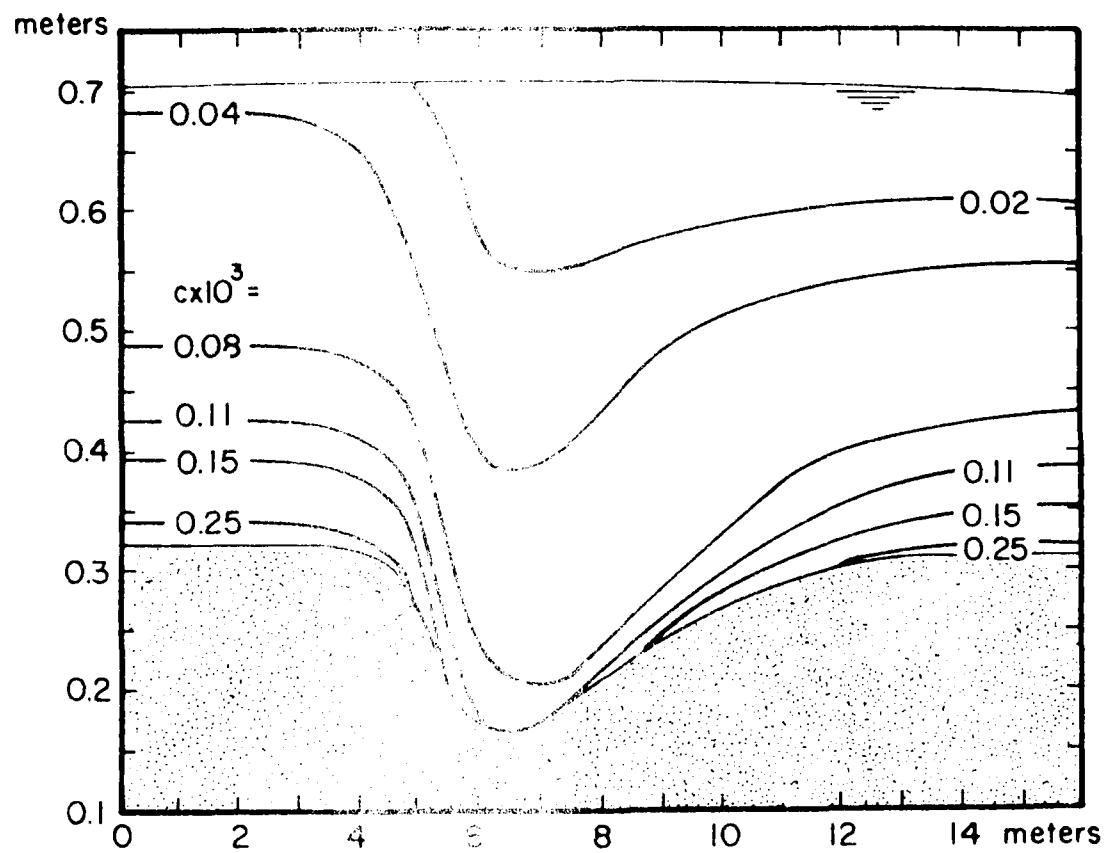


Fig. 13. Distribution of suspended sediment after 7 hours.

5

CONCLUSIONS AND RECOMMENDATIONS

5.1 CONCLUSIONS

1. A two-dimensional numerical model has been developed to predict water and sediment movement and water surface and bed-elevation changes in channel reaches with complex boundary geometry.
2. The model is based on the conservation laws of water and sediment continuity, and momentum equations. The water continuity and momentum equations are solved first. The predicted flow variables are then introduced into transport formulas and the sediment continuity equation to compute sediment load rates and changes in bed elevation, respectively. The equations of motion are solved using a finite-element scheme.
3. The model has been validated by simulating laboratory data obtained from a trench scour and fill study. The model predicts satisfactorily the evolution of the water surface and bed elevations. In another test the model was used to simulate bed scour around a spur dike. The shape of the predicted scour hole is in qualitative agreement with observations reported in the literature. However, the deviations observed in the predicted locations of maximum scour and deposition point out a limitation in the model when simulating situations dominated by regions of flow separation. Further research is needed to correct this deficiency.

5.2 RECOMMENDATIONS

1. It is recommended that the model be further developed and tested on real systems to ensure its accuracy and credibility. Work should continue on the computer code to improve its flexibility and efficiency. Carefully designed laboratory experiments should be conducted to investigate the accuracy and range of applicability of transport algorithms used in the model (i.e., turbulence closure schemes, two-dimensional sediment transport functions, etc.). Two-dimensional models have a great potential to study in detail sediment related problems in irregular stream reaches with significant flow components in more than one direction.

2. Verification and validation of two-dimensional models require data with a degree of detail and spatial resolution that is practically nonexistent. It is thus recommended that laboratory data be collected in scaled down physical models reproducing conditions observed in the field. Laboratory studies can provide, at a reasonable cost, velocity, sediment transport, and cross sectional data with the high degree of resolution needed in model validation. Then, a few carefully selected prototype measurements in the field will suffice for model verification.
3. It is recommended that hypothetical situations be used to confirm that the model responds in a realistic manner. To this effect, the two-dimensional model can be linked to one-dimensional channel and sediment yield models to investigate the dynamic response of local bank stabilization structures to changes in upstream land management practices, and to series of intense storm events. These consolidated models could be used, for instance, to look at (a) bed and bank response in the vicinity of toe armor, hard points, fences, etc.; (b) degree of bank destabilization caused by proximity of point bar; etc.

REFERENCES

Ahmad, M., "Experiments on Design and Behavior of Spur Dikes," Proceedings, Minnesota International Hydraulics Convention, 145-159, 1953.

Alonso, C. V. and Wang, S. Y., "Finite Element Modeling of Flow Around an Open Channel Obstruction," Proceedings, 2nd International Conference of Finite Elements in Water Resources, Imperial College, London, England, 1978.

Alonso, C. V. and Wang, S. Y., "Simulation of Local Scour and Fill in Sandbed Streams," Proceedings, 3rd International Conf. on Finite Elements in Water Resources, The University of Mississippi, 1980.

Argyris, J. H., Mareczek, G. and Scharpf, D. W., "Two and three dimensional flow using finite elements", J. Roy. Aero. Soc., Vol. 73, 961-964, 1969.

Ariathurai, R. and Krone, R. B., "Finite Element Model for Cohesive Sediment Transport," Journal of the Hydraulics Division, ASCE, 1976.

Atkinson, B., Brocklebank, M. P., Card, C. C. H. and Smith, J. M., "Low Reynolds number developing flow," A. I. Ch. E. J., Vol. 15, 548-553, 1969.

Chen, C. L., "Sediment Dispersion in Flow with Moving Boundary," Journal Hydraulics Division, ASCE, Vol. 97, No. HY8 pp 1181-1201, 1971.

Coleman, N. L., "Flume studies of the sediment transfer coefficient," Water Resources Research, Vol. 6, No. 3, 801-809, 1970.

Connor, J. J. and Brebbia, C. A., Finite Element Techniques for Fluid Flow, Newnes-Butterworth, London, 1976.

Cunge, J. A. and Perdreau, N., "Mobile Bed Fluvial Mathematical Models," La Houille Blanche, No. 7, 1973.

DeVries, M., "River Bed Variations-Aggradation and Degradation," Publication No. 17, Delft Hydraulics Laboratory, Delft, The Netherlands, 1973.

Engelund, F., and Hansen, E., A monograph on sediment transport in alluvial streams. Teknisk Forlag, Copenhagen, 1967.

Fredsøe, J., "Meandering and braiding of rivers," Journal of Fluid Mechanics, Vol. 84, Part 4, 609-624, 1978.

Garde, R. J., Subramanya, K., and Nambudripad, K. D., "Study of Scour Around Spur Dikes," Journal of the Hydraulics Division, ASCE, Vol. 87, No. HY6, 23-37, 1961.

Graf, W. H., Hydraulics of Sediment Transport, McGraw-Hill, New York, 1971.

Jobson, H. E. and Sayre, W. W., "Predicting Concentration Profiles in Open Channels," Journal of the Hydraulics Div., ASCE, Vol. 96, No. HY10, pp. 1983-96, 1970.

Katopodes, N. D., "Finite Element Model for Open Channel Flow Near Critical Conditions," Proceedings, 3rd Int. Conf. on Finite Elements in Water Resources, Vol. 2, 5.37-5.46, 1980.

Kerssens, P. J. M., van Rijn, L. C. and van Wijngaarden, J. J., "Model for Non-steady Suspended Sediment Transport," IAHR Modelling of Sediment Transport, pp 113-20, 1977.

Keuning, D. H., "Application of Finite Element Method to Open Channel Flow," Journal of the Hydraulics Division, ASCE, 1976.

Leendertse, J. J., "Aspects of a Computational Model Long-period Water-wave Propagation," Rand Corp. Memorandum, RM-5294-PR, 1967.

Leimkuhler, W. et al., "Two-Dimensional Finite Element Dispersion Model," Proc. Symposium on Modeling techniques, Vol. II, 1975.

Lopez, S. J. L., "Mathematical Modeling of Sediment Deposition in Reservoirs," Hydrology Paper No. 95, CSU, Fort Collins, Colorado, July, 1978.

Luke, J. C., "A variational principle for a fluid with a free surface," J. Fluid Mech., Vol. 27, p. 395, 1967.

Mahmood, K., "Mathematical Modeling of Morphological Transients in Sandbed Canals," International Association for Hydraulic Research, 1974.

Mahmood, K., "Mathematical modeling of morphological transients in sandbed canals," Proceedings, Sixteenth Congress of the International Association for Hydraulic Research, Vol. 2, 57-64, 1975.

Martin, H. C., "Finite element analysis of fluid flows," Proc. 2nd Conf. Matrix Methods in Structural Mechanics, Wright Patterson AFB, Ohio, AFFDL-TR-68-150, 1968.

Nakayama, P. I. and Romero, N. C., "Numerical Method for Almost 3-D Incompressible Fluid Flow and a Simple Internal Obstacle," J. of Computational Physics, Vol. 8, 230-40, 1971.

Niemeyer, G. L., "Numerical Method for the Simulation of Hydrodynamic and Ecological Processes, with Application to Kaneohe Bay, Oahu, Hawaii," 1977.

Norrie, D. H. and deVries, G., "A Survey of the finite element applications in fluid mechanics, Finite Elements in Fluids," Vol. 3, 363-84, 1978.

O'Carroll, M. J., "Complementary variational principles for steady ideal flows with free surfaces," J. Fluid Mechanics, 1975.

O'Carroll, M. J., "A variational principle for ideal flow over a spillway," submitted to Int. J. Numer. Meth. Eng., 1975a.

O'Carroll, M. J. and Harrison, H. T., "Variational techniques for free-streamline problems," Proceedings, 2nd Int. Symp. Finite Element Methods in Flow Problems, Genoa, 1976.

O'Carroll, M. J., "Variational Methods for Free Surfaces of Cavitation, Jets, Open Channel Flows, Separation, and Wakes," Finite Elements in Fluid Flow, Vol. 3, 293-308, 1978.

Oden, J. T. and Sornogyi, D., "Finite element applications in fluid dynamics," J. Eng. Mech. Div., A.S.C.E., Vol. 95, No. EM3, 821-826, 1969.

Oden, J. T., "Finite element analogue of Navier-Stokes equations," J. Eng. Mech. Div., A.S.C.E., Vol. 96, No. EM4, 529-534, 1970.

Oden, J. T. and Wellford, Jr., L. C., "Analysis of flow of viscous fluids by the finite element method," AIAA J., Vol. 10, No. 12, 1590-1599, 1972.

Olson, M. D., "A variational finite element method for two-dimensional steady viscous flows," McGill-EIC Conf. on Fin. Elem. Meth. in Civ. Eng., Montreal, June 1-2, 1972.

Olson, M. D., "Variational-finite element methods for two-dimensional and axisymmetric Navier-Stokes equations", Finite Elements in Fluids, Vol. 1, 57-71, 1975.

Simons, D. B., Richardson, E. V., and Mahmood, K., "One-Dimensional Modeling in Alluvial River Flow," Chap. 19 of Proc. on Unsteady Flow in Open Channel, WRP, 1975.

Simons, D. B., Chen, Y. H., and Ponce, V. M., "Development of a 2-D Water and Sediment Routing Model and its Application to Study Lower Pool 4 and in the Upper Mississippi River System," Colorado State University, 1979.

Skiba, E., "A finite element solution of general fluid dynamics problems-natural convection in rectangular cavities", M. App. Sci. Civ. Eng. Thesis, University of Waterloo, Ontario, Canada, 1970.

Smith, T. J. and O'Connor, B. A., "A Two-Dimensional Model for Suspended Sediment Transport," Proceedings, IAHR 17th Congress, Vol. 1, pp 79-87, 1977.

Su, T. Y., Wang, S. Y., and Alonso, C. V., "Depth-Averaging Models of River Flows", Proceedings, 3rd Int. Conf. on Finite Elem. in Water Resources, University of Mississippi, 1980.

Thienpont, M. and Berlamont, J., "A Finite Element Solution For Depth-Averaged Two-Dimensional Navier-Stokes Equations For Flows in Rivers and Channels", Proceedings, 3rd Int. Conf. on Finite Elem. in Water Resources, Vol. 2, 5.28-5.36, 1980.

Tong, P., "The finite element method for fluid flow", Japan-U.S. Seminar on Matrix Methods of Structural Analysis and Design, Tokyo, Japan, 1969.

Vries, M. de, "Application of Physical and Mathematical Models for river Problems," Symposium on River Mechanics IAHR Bangkok, 1973.

Yang, C. T., and Sayre, W. W., "Longitudinal Dispersion of Bed Material Particles," Journal Hydraulics Div., ASCE, Vol. 97, No. HY7, pp 907-21, 1971.

Zaghloul, N. A., and McCorquodale, J. A., "A Stable Numerical Model for Local Scour," Journal of Hydraulic Research, Vol. 13, No. 4, 425-444, 1975.

ADDENDUM 1: DERIVATION OF TWO-DIMENSIONAL DEPTH-AVERAGED FLOW EQUATIONS

The fluid flow in a natural stream is always turbulent, three-dimensional and time-dependent. In many instances, however, the flow is predominantly horizontal. That is, the flow velocity in both the longitudinal and transverse directions are comparable and much larger than the vertical velocity component. In such cases, an expedient approximation to the three-dimensional flow problem is to assume bidimensionality along the two perpendicular horizontal directions, averaging flow properties in the vertical direction. The pressure distribution along the vertical is assumed hydrostatic, only time-averaged turbulent flow notions are considered, and the effects of small-scale velocity fluctuations are aggregated into the shear stress terms.

Continuity equation of water and Navier-Stokes Equation are written

$$\frac{\partial \bar{u}}{\partial t} + \frac{\partial \bar{u}^2}{\partial x} + \frac{\partial \bar{v}\bar{u}}{\partial y} + \frac{\partial \bar{w}\bar{u}}{\partial z} + \frac{1}{\rho} \frac{\partial \bar{p}}{\partial x} - \frac{1}{\rho} (\frac{\partial \bar{\tau}_{xx}}{\partial x} + \frac{\partial \bar{\tau}_{xy}}{\partial y} + \frac{\partial \bar{\tau}_{xz}}{\partial z}) = 0 \quad (1.1)$$

$$\frac{\partial \bar{v}}{\partial t} + \frac{\partial \bar{u}\bar{v}}{\partial x} + \frac{\partial \bar{v}^2}{\partial y} + \frac{\partial \bar{w}\bar{v}}{\partial z} + \frac{1}{\rho} \frac{\partial \bar{p}}{\partial y} - \frac{1}{\rho} (\frac{\partial \bar{\tau}_{yx}}{\partial x} + \frac{\partial \bar{\tau}_{yy}}{\partial y} + \frac{\partial \bar{\tau}_{yz}}{\partial z}) = 0 \quad (1.2)$$

$$\frac{\partial \bar{p}}{\partial z} + \rho g = 0 \quad (1.3)$$

$$\frac{\partial \bar{u}}{\partial x} + \frac{\partial \bar{v}}{\partial y} + \frac{\partial \bar{w}}{\partial z} = 0 \quad (1.4)$$

where x , y are longitudinal and transverse horizontal coordinates, z is the vertical coordinate measured upwards from arbitrary datum, t is time, \bar{u} , \bar{v} , and \bar{w} are time-averaged velocity components in x , y , z directions, ρ is density, \bar{p} is time-averaged pressure, g is acceleration of gravity, and $\bar{\tau}_{ij}$ is the time-averaged shear stress in the j th-direction on a plane normal to the i th-axes.

The assumed boundary conditions are

1. the pressure on the free surface is taken as constant.
2. the free surface shear stress is neglected.
3. the fully developed flow is imposed at the upstream.
4. no slip, no seepage on the channel wall and bed.

Then they can be translated into the mathematical formulations,

$$z = \rho(x, y), \bar{u} = \bar{v} = \bar{w} = 0 \quad \text{on the bottom} \quad (1.5)$$

$$z = \eta(x, y), \bar{p} = \bar{p}_o \quad \text{on the free surface} \quad (1.6)$$

$$-\bar{\tau}_{xx} \frac{\partial \eta}{\partial x} - \bar{\tau}_{xy} \frac{\partial \eta}{\partial y} + \bar{\tau}_{xz} = \bar{\tau}_x^s \quad (1.7)$$

$$-\bar{\tau}_{xy} \frac{\partial \eta}{\partial x} - \bar{\tau}_{yy} \frac{\partial \eta}{\partial y} + \bar{\tau}_{yz} = \bar{\tau}_y^s$$

where $\bar{\tau}_x^s, \bar{\tau}_y^s$ are the surface wind stresses. Similar expression holds for bed shear stresses.

Eqn. 1.3 yields:

$$\int_z^\eta \frac{\partial \bar{p}}{\partial z} dz = - \int_z^\eta \rho g dz$$

from which:

$$\bar{p} = \bar{p}_o + \rho g(\eta - z) \quad (1.8)$$

Applying vertical integration, using the Leibnitz's rule, and Eqn. 1.8, the Navier-Stoke's equations can be transformed into Eqns. 1.9-1.12 shown below.

The x -momentum equation becomes

$$\begin{aligned} \frac{\partial \langle u \rangle}{\partial t} - u(x, y, \eta, t) \frac{\partial \eta}{\partial t} + u(x, y, \zeta, t) \frac{\partial \zeta}{\partial t} + \frac{\partial \langle u^2 \rangle}{\partial x} - [u(x, y, \eta, t)]^2 \frac{\partial \eta}{\partial x} \\ + [u(x, y, \eta, t)]^2 \frac{\partial \zeta}{\partial x} + \frac{\partial \langle uv \rangle}{\partial y} - u(x, y, \eta, t) v(x, y, \eta, t) \frac{\partial \eta}{\partial y} \\ + u(x, y, \zeta, t) v(x, y, \zeta, t) \frac{\partial \zeta}{\partial y} + u(x, y, \eta, t) w(x, y, \eta, t) - \\ u(x, y, \zeta, t) w(x, y, \zeta, t) + g \left\langle \frac{\partial \eta}{\partial x} \right\rangle - \frac{1}{\rho} \left\{ \frac{\partial \langle \tau_{xx} \rangle}{\partial x} - \right. \\ \left. \tau_{xx}(x, y, \eta, t) \frac{\partial \eta}{\partial x} + \tau_{xx}(x, y, \zeta, t) \frac{\partial \zeta}{\partial x} + \frac{\partial \langle \tau_{xy} \rangle}{\partial y} - \right. \\ \left. \tau_{xy}(x, y, \eta, t) \frac{\partial \eta}{\partial y} + \tau_{xy}(x, y, \zeta, t) \frac{\partial \zeta}{\partial y} + \left\langle \frac{\partial \tau_{xz}}{\partial z} \right\rangle \right\} = 0 \quad (1.9) \end{aligned}$$

$$\begin{aligned}
& \frac{\partial(hU)}{\partial t} + \frac{\partial(hU^2)}{\partial x} + \frac{\partial(hUV)}{\partial y} - u(\eta) \left[\frac{\partial \eta}{\partial t} + u(\eta) \frac{\partial \eta}{\partial x} + v(\eta) \frac{\partial \eta}{\partial y} \right] + \\
& u(\rho) \left[\frac{\partial \rho}{\partial t} + u(\rho) \frac{\partial \rho}{\partial x} + v(\rho) \frac{\partial \rho}{\partial y} \right] + u(\eta) w(\eta) - u(\rho) w(\rho) \\
& + gh \frac{\partial \eta}{\partial x} - \frac{1}{\rho} \frac{\partial \tau_{xx}}{\partial x} - \frac{1}{\rho} \frac{\partial \tau_{xy}}{\partial y} - \frac{1}{\rho} [\tau_{xy}(\eta) - \tau_{xy}(\eta) \frac{\partial \eta}{\partial y}] \\
& - \tau_{xx}(\eta) \frac{\partial \eta}{\partial x} + \frac{1}{\rho} [\tau_{xz}(\rho) - \tau_{xy}(\rho) \frac{\partial \rho}{\partial y} - \tau_{xx}(\rho) \frac{\partial \rho}{\partial x}] = 0
\end{aligned}$$

Imposing the boundary conditions, Eqns. 1.5-1.7, we have

$$\begin{aligned}
& \frac{\partial(hU)}{\partial t} + \frac{\partial(hU^2)}{\partial x} + \frac{\partial(hUV)}{\partial y} + gh \frac{\partial \eta}{\partial x} - \frac{1}{\rho} \frac{\partial(hT_{xx})}{\partial x} - \frac{1}{\rho} \frac{\partial(hT_{xy})}{\partial y} \\
& - \frac{1}{\rho} (\tau_x^s - \tau_x^b) = 0
\end{aligned} \tag{1.10}$$

In a similar fashion the Y-momentum equation yields

$$\begin{aligned}
& \frac{\partial(hV)}{\partial t} + \frac{\partial(hUV)}{\partial x} + \frac{\partial(hV^2)}{\partial y} + gh \frac{\partial \eta}{\partial y} - \frac{1}{\rho} \frac{\partial(hT_{xx})}{\partial x} - \frac{1}{\rho} \frac{\partial(hT_{yy})}{\partial y} \\
& - \frac{1}{\rho} (\tau_y^s - \tau_y^b) = 0
\end{aligned} \tag{1.11}$$

Finally, the continuity equation yields

$$\begin{aligned}
& \frac{\partial(u)}{\partial x} - u(\eta) \frac{\partial \eta}{\partial x} + u(\zeta) \frac{\partial \zeta}{\partial x} + \frac{\partial(v)}{\partial y} - v(\eta) \frac{\partial \eta}{\partial y} + v(\zeta) \frac{\partial \zeta}{\partial y} \\
& + w(\eta) - w(\zeta) = 0 \\
& \frac{\partial(hU)}{\partial x} + \frac{\partial(hV)}{\partial y} + [w(\eta) - u(\eta) \frac{\partial \eta}{\partial x} - v(\eta) \frac{\partial \eta}{\partial y}] - [w(\zeta) - \\
& u(\zeta) \frac{\partial \zeta}{\partial x} - v(\zeta) \frac{\partial \zeta}{\partial y}] = 0 \\
& \frac{\partial(hU)}{\partial x} + \frac{\partial(hV)}{\partial y} + \frac{\partial h}{\partial t} - \frac{\partial \zeta}{\partial t} = 0 \\
& \frac{\partial(hU)}{\partial x} + \frac{\partial(hV)}{\partial y} + \frac{\partial h}{\partial t} = 0
\end{aligned} \tag{1.12}$$

ADDENDUM 2

COMPUTER PROGRAM OF DEPTH-AVERAGED FLOW MODEL

C

MAIN PROGRAM FOR SOLVING DEPTH-AVERAGED FLOW AND SEDIMENT PROBLEM

PARAMETER NNG=378, NIT=104, NRT=13, NCK=8, NMK=283, NJK=96

PARAMETER NRT1=126, NRT2=14

PARAMETER DELTAZ=3000., CGX=0.013, CGY=0.013, POROSE=0.45

PARAMETER N51=65, NB1H=32, NE2=57, NB2H=28

PARAMETER NE3=21, NB3H=10

PARAMETER RN=1.0, GRAV=32.2, COEF=0.005

DIMENSION ZX(15),ZY(15),ZB(15),ZV(15),SED(15),GUESS(15)

DIMENSION I2(NMK),I22(NMK),GR1(NNG),GR2(NNG),R1(NMK),R2(NNG)

DIMENSION SGX(NNG1),SGY(NNG1),SLH(NNG1,NB3),SRB(NNG1)

FLUX(NRT1),F1(NNG),F2(NNG),DELTAF(NNG)

PSI(NMK),C2(NMK,1),XL(8207),RHA(NMK),GRH(NNG)

F(NNG,NE1),C1(NMK,NB2)

DIMENSION X(NNG),Y(NNG),Z(NNG),DELTAZ(NNG)

GX(4),GY(4),XX(4),YY(4),II(4)

DJ(4),VI1(4),VI12(4),VI21(4),VI22(4)

AF1(4,4),AF1X(4,4),AF1Y(4,4),AF1B(4,4)

DATA XX/-1.'1.-1.'1./

DATA GX/0.57735,0.57735,-0.57735,-0.57735/

DATA GY/0.57735,-0.57735,0.57735,-0.57735/

READ(15,1010) ZX

READ(15,201) (X(K),K=1,NNG,3)

READ(15,1010) ZY

READ(15,201) (Y(K),K=1,NNG,3)

FORMAT(1X,9F8.3)

READ(15,1010) ZB

READ(15,202) (I22(I),I=1,NMK)

FORMAT(1X,9I7)

CALL NODGEN(NMK,NMK,I22,I2)

READ(15,1010) ZV

READ(15,203) (PSI(I),I=1,NMK)

FORMAT(1X,9F7.3)

READ(16,1010) RED

READ(16,901) (Z(I),I=3,NNG,3)

READ(16,1010) GUESS

READ(16,901) (GR2(I),I=1,NNG)

201
202
203

```

ITERT=0
ITERT=ITERT+1
DO 5099 I=3,NNG,3
F1(I)=GR2(I)+Z(I)
CONTINUE
ITER=0
ITER=ITER+1
DO 506 I=1,NEK
R1(I)=0.
DO 506 J=1,NB2
C1(I,J)=0.
CONTINUE
DO 505 I=1,NIG
GRH(I)=GR2(I)
A2(I)=0.
DO 505 J=1,NE1
F(I,J)=0.
CONTINUE
DO 100 IE=1,NCT
IC=(IE-1)/NCT+1
IR=IE-(IC-1)*NCT
II(1)=1+3*IR+3*(IC-1)*(NCT+1)
II(2)=II(1)+3*(IC-1)
II(3)=II(1)-3
II(4)=II(2)-3
DO 100 KK=1,4
VJ11=0.
VJ12=0.
VJ22=0.
VJ21=0.
DO 150 N=1,4
AF1(N,KK)=(1.+XX(K))*GX(KK)*(1.+YY(N))*GY(KK))/2.
AF1X(N,KK)=XX(K)*(1.+YY(N))*GY(KK))/4.
AF1Y(N,KK)=YY(N)*(1.+XX(N))*GX(KK))/4.
AF1B(K,KK)=(1.+YY(K))*GY(KK))/2.

```

150

VJ11=VJ11+AF1X(K, KK)*X(I1(K))
VJ12=VJ12+AF1X(K, KK)*Y(I1(K))
VJ21=VJ21+AF1Y(K, KK)*X(I1(K))
VJ22=VJ22+AF1Y(K, KK)*Y(I1(K))

CONTINUE

DJ(KK)=VJ11*VJ22-VJ12*VJ21

VII1(KK)=VJ22/DJ(KK)

VII2(KK)=-VJ12/DJ(KK)

VII3(KK)=-VJ21/DJ(KK)

VII4(KK)=VJ11/DJ(KK)

GO TO 115
IF (IE .LE. NCT*(WRT-1)) GO TO 115

IF (KK .GE. 3) GO TO 115

DO 117 N=2,4,2

I=II(K)

J=II(N-1)

I1=I+1

J1=J+1

H=-AF1B(K, KK)*VJ22

GRH(I)=GRH(I)+GR1(1+2)*RN#H*(GR1(J)-GR1(I))/(X(J)-X(I))

GRH(I1)=GRH(I1)+GR1(I+2)*RN#H*(GR1(J1)-GR1(I1))/(X(J)-X(I))

CONTINUE

117 DO 112 N=1,4

SUM1=0.

SUM2=0.

DO 113 I=1,4

I=II(K)

I1=I+1

J=II(N)

H=-AF1(K, KK)*(AF1X(K, KK)*VII1(K, KK)+AF1Y(K, KK)*VII2(KK))

1 #Z(J+2)*D2(KK)

G=-AF1(K, KK)*(AF1X(K, KK)*VII21(KK)+AF1Y(K, KK)*VII22(KK))

1 #Z(J+2)*D2(KK)

SUM1=SUM1+H*GRAV*CR1(I+2)

SUM2=SUM2+G*GRAV*CR1(I+2)

CONTINUE

113


```

104      F(I,J1)=F(I,J1)+B1*GRAV*GR1(I)
      CONTINUE
      DO 105 N=1,4
      DO 105 M=1,4
      I=II(N)+2
      J=II(E)+1
      CA=(AF1X(M,KK)*VI11(KK)+AF1Y(M,KK))*VI22(KK)*AF1(N,KK)*DJ(KK)
      J1=J-I+NE1H+1
      F(I,J1)=F(I,J1)+CA*GRAV*GR1(I)
      CONTINUE
      DO 106 N=1,4
      DO 106 M=1,4
      I=II(N)+2
      J=II(E)+2
      B2=(AF1X(M,KK)*VI11(KK)+AF1Y(M,KK))*VI12(KK)*AF1(N,KK)*DJ(KK)
      C   1   CB=(AF1X(M,KK)*VI21(KK)+AF1Y(M,KK))*VI22(KK)*AF1(N,KK)*DJ(KK)
      C   1   AF1(L,KK)
      J1=J-I+NE1H+1
      F(I,J1)=F(I,J1)+B2*GRAV*GR1(I-2)+CB*GRAV*GR1(I-1)
      CONTINUE
      DO 107 N=1,4
      DO 107 M=1,4
      I=II(N)
      J=II(E)+2
      B1=(AF1X(M,KK)*VI11(KK)+AF1Y(M,KK))*VI12(KK)*AF1(N,KK)*DJ(KK)
      J1=J-I+NE1H+1
      F(I,J1)=F(I,J1)+B1*GR1(I+2)*GR1V
      CONTINUE
      DO 108 N=1,4
      DO 108 M=1,4
      I=II(E)+1
      J=II(E)+2
      C=(AF1X(M,KK)*VI21(KK)+AF1Y(M,KK))*VI22(KK)*AF1(N,KK)*DJ(KK)
      J1=J-I+NE1H+1
      F(I,J1)=F(I,J1)+C*GR1(I+1)*GR1V

```

```

100  CONTINUE
      DO 111 I=1,4
      DO 111 J=1,4
      SUM=C.
      DO 111 L=1,4
      L=I*I(L)+1
      L=L*(L)
      C=(AF12(L,MN)*V111(MN)+AF12(L,MN)*V122(MN))*G11(L)
      AF11(L,MN)=AF11(L,MN)+SUM
      111  SUM=SUM+C
      CONTINUE
      J1=J-I+M2*I+1
      F(I,J1)=F(I,J1)+SUM*G11(I+L)
      111  CONTINUE
      DO 110 I=1,4
      DO 110 J=1,4
      SUM=C.
      DO 110 L=1,4
      L=I*I(L)+1
      L=L*(L)
      C=(AF12(L,MN)*V111(MN)+AF12(L,MN)*V122(MN))*G11(L)
      AF11(L,MN)=AF11(L,MN)+SUM*G11(I+L)
      110  SUM=SUM+C
      CONTINUE
      J1=J-I+M2*I+1
      F(I,J1)=F(I,J1)+SUM*G11(I+1)
      110  CONTINUE
      DO 32 I=1,MNG
      SUM(I)=C.
      DO 32 J=1,M51
      IF ( F(I,J) .EQ. 0. ) GO TO 32
      J1=I-M2*I-1+J
      RHA(I)=RHA(I)+F(I,J)*G11(J1)

```

```

39      CONTINUE
      RHA(I)=RHA(I)+GRH(I)
      CONTINUE
      DO 31 I=1,NKH
      DO 31 J=1,NKH
      L4=I2(I)
      L5=I2(J)
      IF ( IADS(L4-L5) .GT. NE1H ) GO TO 31
      L6=L5-L4+1+N51H
      J1=J-(I-1)+N52H
      IF ( J1 .GT. N52 ) GO TO 31
      C1(I,J1)=F(L4,L6)
      CONTINUE
      CALL LEQT1B(C1,NKH,NB2H,N52E,NKH,C2,1,NKH,1,XL,IER)
      DO 300 I=1,NKH
      C2(I,1)=0.
      CONTINUE
      DO 301 I=1,NKH
      C2(I,1)=1.0
      J1=I2(I)
      CALL LEQT1S(C1,NKH,NB2H,NE2H,NKH,C2,1,NKH,2,XL,IER)
      DO 303 J=1,NKH
      R1(J)=R1(J)+C2(J,1)*RHA(J1)
      C2(J,1)=0.
      CONTINUE
      DO 305 I=1,NKH
      L4=I2(I)
      R2(L4)=R1(I)
      CONTINUE
      DO 313 I=1,NKH
      GR2(I)=GR1(I)-R2(I)
      CONTINUE
      WRITE(17,801) ITER
      FORMAT(1H1,1X,'ITER=' ,15)
      DO 601 I=1,3

```

```

      WRITE(17,700)
      FORMAT(1X,/)

      WRITE(17,701) (GR2(J),J=1,MIG,3)
      FORMAT(1X,9E13.5)

CONTINUE
      IF (ITER .GT. 1 ) GO TO 504
      DO 501 I=1,MIG,3
      IF ( ABS(GR1(I)) .LE. 0.0010 ) GO TO 501
      IF ( ABS(1.-GR2(I))/GR1(I) .GT. :01 ) GO TO 502
CONTINUE
      IF (ITER .EQ. 1 ) GO TO 502
      GO TO 504

502   TYPE 1001,1
      FORMAT(1X,I10)
      TYPE 1002,ITER
      FORMAT(1X,I15)
      GO TO 500
      DO 3001 I=1,MIG,3
      N=(GR2(I)**2.+GR2(I+1)**2.)**0.5
      L=I/3+1
      SGX(L)=CGX*GR2(I)**3.6
      SGY(L)=CGY*GR2(I+1)**3.6
CONTINUE
      DO 3002 IE=1,MIG
      IF ( IE .GT. 44 .AND. IE .LT. 49 ) GO TO 3002
      NC=(IE-1)/MCT+1
      NF=IE-(NC-1)*MCT
      II(1)=1+3*MIG+3*(NC-1)*(MCT+1)
      II(2)=II(1)+3*(MCT+1)
      II(3)=II(1)-3
      II(4)=II(2)-3
      DO 3002 KK=1,4
      VJ11=0.
      VJ12=0.
      VJ22=0.
      VJ21=0.

```

```

DO 3003 H=1,4
AF1(X,KK)= (1.+XX(H))*GX(KK))*(1.+YY(H))*GY(KK))/4.
AF1X(H,KK)= XX(H)*(1.+YY(H))*GY(KK))/4.
AF1Y(H,KK)= YY(H)*(1.+XX(H))*GX(KK))/4.
VJ11=VJ11+AF1X(H,KK)*Y(II(H))
VJ12=VJ12+AF1X(H,KK)*Y(II(H))
VJ21=VJ21+AF1Y(H,KK)*Y(II(H))
VJ22=VJ22+AF1Y(H,KK)*Y(II(H))

3003  CONTINUE
DJ(KK)=VJ11*VJ22-VJ12*VJ21
VI11(KK)=VJ22/DJ(KK)
VI12(KK)=-VJ12/DJ(KK)
VI21(KK)=-VJ21/DJ(KK)
VI22(KK)=VJ11/DJ(KK)
DO 3004 H=1,4
SUM=0.
DO 3005 H=1,4
I=II(H)/3+1
J=II(H)/3+1
J1=II(H)
B=-AF1(H,KK)*(AF1X(H,KK)*VI11(KK)+AF1Y(H,KK)*VI12(KK))*DJ(KK)
C=-AF1(H,KK)*(AF1X(H,KK)*VI21(KK)+AF1Y(H,KK)*VI22(KK))*DJ(KK)
D=(1.0-POROS)*GRAV*AF1(H,KK)*AF1(H,KK)*DJ(KK)/DELTAT
SUM=SUM+B*SGW(J)+C*SGY(J)+D#2*(J1+2)
J2=J-I+KE3H+1
SLH(I,J2)=SLH(I,J2)+D
3005  CONTINUE
SRE(I)=SRH(I)+SUM
CONTINUE
3004
3002  CONTINUE
CALL SOLVEA(SLR,SRH,HNG1,HNG2)
WRITE(20,901) (SRH(I),I=1,HNG1)
OPEN (UNIT=19,ACCESS='SEQUENTIAL')
WRITE(19,901) (SRE(I),I=1,HNG1)
FORMAT(1X,9516.2)
CLOSE (UNIT=19)

```

```

DO 3008 I=3,NNG,3
L=I/3
DELTAZ(I)=SRH(L)-Z(I)
Z(I)=SRH(L)
SRH(L)=0.
DO 3008 J=1,RB3
SLH(L,J)=0.
CONTINUE
DO 310 I=1,NRT1
FLUX(I)=0.
DO 310 J=1,NCT
L1=(J-1)+(I-1)*(NCT+1)*3+1
L2=L1+3
1
FLUX(I)=FLUX(I)+(Y(L2)-Y(L1))*(GR2(L2)*GR2(L2+2)
+GR2(L1)*GR2(L1+2))/2.
F2(L1+2)=GR2(L1+2)+Z(L1+2)
DELTAF(L1+2)=F2(L1+2)-F1(L1+2)
CONTINUE
WRITE(17,7C2) (FLUX(I),I=1,NRT1)
WRITE(17,7C1) (DELTAF(I),I=3,NNG,3)
702 FORMAT(1X,14E13.5)
WRITE(20,901) (DELTAZ(I),I=3,NNG,3)
IF (ITERT.GT. 2 ) GO TO 508
GO TO 509
508 WRITE(18,901) (Z(I),I=3,NNG,3)
WRITE(18,901) (GR2(I),I=1,NNG)
1210 FORMAT(15A3)
STOP
END
SUBROUTINE NODGEN(MKV,MVK,I11,I1)
DIMENSION I11(MVK),I1(MVK)
I=1
I=0
DO 8 J=1,MVK
K=I11(J)
I=I+1
8

```

IF (M .GE. K) GO TO 8
I1(I)=M
I=I+1
GO TO 9
CONTINUE
RETURN
END

SUBROUTINE SOLVEA(SK,R1,NEQ,NBAND)
DIMENSION SK(NBAND),R1(NEQ).
NBANDH=(NBAND+1)/2
DO 300 N=1 ,NEQ
L1=N+1
L2=N+NBANDH-1
N2=NBANDH
DO 290 N1=L1,L2
IF (L1 .GT. NEQ) GO TO 290
N1=NBANDH
N2=N2-1
IF (SK(N1,N2) .EQ. 0.) GO TO 290
C=SK(N1,N2)/SK(N,N1)
N5=N2
DO 270 N3=N1+1,NBAND
N5=N5+1
IF (SK(N,N3) .EQ. 0.) GO TO 270
SK(N1,N5)=SK(N1,N5)-C*SK(N,N3)
CONTINUE
R1(N1)=R1(N1)-C*R1(N)
CONTINUE
J=N-(N-NBANDH-1)
J1=J-1+NBAND-NBANDH
DO 260 N4=J,J1
SK(N,N4)=SK(N,N4)/SK(N,N1)
CONTINUE
R1(N)=R1(N)/SK(N,N1)
CONTINUE
N=NEQ

350 K=N-1
 IF (N) 500,500,360
 K1=NBANDH
 L=N
 DO 400 K=K1+1,NENDD
 L=L+1
 IF (L .GT. NEQ) GO TO 400
 IF (SK(,,K)) 370,400,370
 R1(R)=R1(R)-SK(R,K)*R1(L)
 CONTINUE
 GO TO 350
 RETURN
 END

